Journal of Hepatocellular Carcinoma

Dovepress
Taylor & Francis Group

Open Access Full Text Article

ORIGINAL RESEARCH

BRAP Promotes the Tumorigenesis of Hepatocellular Carcinoma by Corrupting Cancer Cell Cycle Regulation and Enhancing Immune Evasion

Yan Guo[1,*], Ruixue Gu[1,*], Fangmiao Gao[1,*], Lina Liu[1], Dongfeng Deng[2], Qinyu Zhang[1], Longhao Wang[1], Qinglin Liu[3], Ling Lan[4], Shundong Cang[1]

[1]Department of Oncology, Zhengzhou University People's Hospital, Henan Provincial People' s Hospital, Zhengzhou, Henan, People's Republic of China; [2]Department of Hepatobiliary surgery, Zhengzhou University People's Hospital, Henan Provincial People' s Hospital, Zhengzhou, Henan, People's Republic of China; [3]The First Clinical School, Tongji Medical College of Huazhong University of Science & Technology, Wuhan, Hubei, People's Republic of China; [4]Department of Gastroenterology and Hepatology, Zhengzhou University People's Hospital, Henan Provincial People's Hospital, Zhengzhou, People's Republic of China

*These authors contributed equally to this work

Correspondence: Ling Lan, Department of Gastroenterology and Hepatology, Zhengzhou University People's Hospital, Zhengzhou, Henan Province, People's Republic of China, Email lanling@zzu.edu.cn; Shundong Cang, Department of Oncology, Zhengzhou University People's Hospital, Zhengzhou, Henan Province, People's Republic of China, Email shundongcang@zzu.edu.cn

Background: BRAP, a BRCA1-binding protein, exhibits elevated expression across multiple cancers and correlates with poor prognosis in hepatocellular carcinoma (HCC). However, its precise mechanistic roles in HCC tumorigenesis and immune landscape remodeling remain undefined.

Methods: BRAP expression levels and its diagnostic/prognostic value in HCC were analyzed using clinical HCC tissues and public datasets (TCGA and ICGC). CCK-8, colony formation, and EdU assays were employed to evaluate BRAP's impact on HCC cell proliferation; these findings were further validated in vivo using CDX models. RNA-seq and TCGA data analyses were performed to identify BRAP-mediated cellular biological functions and potential underlying mechanisms, with further confirmed via flow cytometry and Western blotting. scRNA-seq data from the GEO and TCGA were used to assess correlations between BRAP expression and immune cell infiltration, as well as immune checkpoint genes (ICGs) expression in HCC. mfIHC, qRT–PCR, and macrophage-tumor co-cultivation experiments were conducted to validate BRAP's regulatory effects on immunosuppressive cell components in HCC.

Results: BRAP expression is significantly upregulated in HCC tissues and correlates with advanced pathological grades and poor patient prognosis. BRAP knockdown markedly reduced HCC cell proliferation both in vitro and in vivo; this anti-proliferative effect was achieved by inducing cell cycle arrest via suppression of the RAF/MEK/ERK signaling pathway. HCC cells with high BRAP expression exhibited increased infiltration of immunosuppressive cells, upregulated ICGs expression, and promoted M2 macrophage polarization.

Conclusion: BRAP drives HCC progression by promoting proliferation via RAF/MEK/ERK and shaping an immunosuppressive microenvironment. We identify BRAP as a novel prognostic biomarker and promising immunotherapeutic target in HCC.

Keywords: hepatocellular carcinoma, BRAP, immune evasion, cell cycle, MAPK/ERK pathway

Introduction

Hepatocellular carcinoma (HCC) is a malignancy characterized by a high incidence and mortality rate worldwide; it is the third leading causing of cancer-related death.[1] Unfortunately, the symptoms of early-stage HCC are not readily apparent. Clinical manifestations typically arise in the intermediate to advanced stages, at which point surgery is not an option. In recent years, novel targeted therapies and immune checkpoint blockade (ICB) therapies have been developed,

Received: 16 June 2025
Accepted: 22 November 2025
Published: 16 December 2025

Graphical Abstract

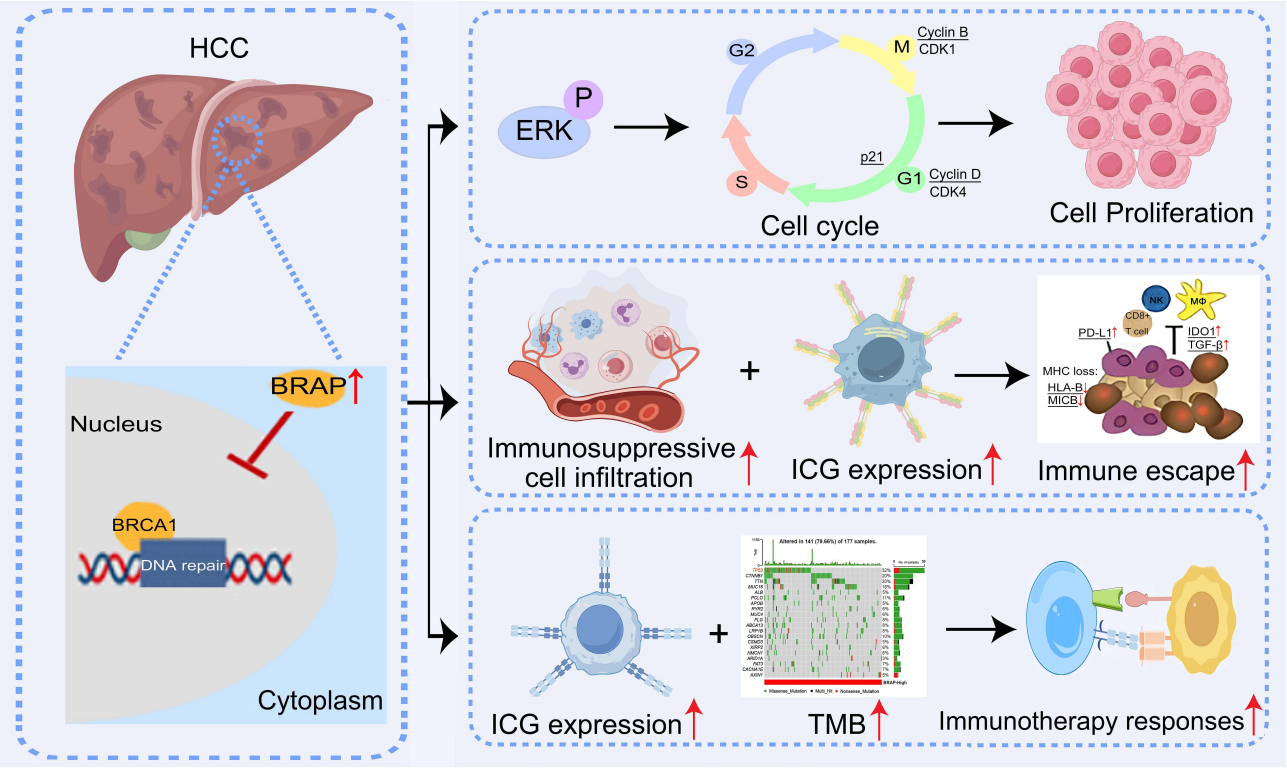

leading to significant advancements in the treatment of advanced HCC. These innovations have markedly increased patient survival rates; however, overall clinical efficacy remains suboptimal.[2–4] Consequently, there is an urgent need for comprehensive exploration of biomarkers that can facilitate early diagnosis, prognosis evaluation, and prediction of therapy outcomes in HCC patients. Such efforts could improve the prognosis and potentially prolong the survival of HCC patients.

BRAP (BRCA1-associated protein) was initially identified through its binding to BRCA1's nuclear localization signal, leading to cytoplasmic retention of BRCA1.[5] Structurally, BRAP contains two functionally important domains: an N-terminal E3 ubiquitin ligase domain and a C-terminal domain that regulates nuclear translocation. This conserved E3 ubiquitin ligase participates in a wide range of biological processes, including cell growth, differentiation, senescence, and inflammation. Mechanistically, BRAP regulates cellular localization and expression of the CDK inhibitor p21 by binding to its nuclear localization signal (NLS). This interaction impairs CDK-cyclin complex activity, thereby disrupting cell cycle progression. Additionally, BRAP modulates the MAPK, NF-κB signaling pathway via ubiquitination-dependent interactions with RAF1 and IKKβ.[6–9] BRAP is an emerging oncogene characterized by overexpression and poor prognosis in cancers including HCC.[10–13] The occurrence and development of HCC involves both tumor-intrinsic transformation and dynamic immune microenvironment crosstalk. Although BRAP critically promotes cancer cell proliferation and invasion, its precise oncogenic mechanisms in HCC, particularly how it mechanistically shapes immune landscape, remain uncharacterized. This knowledge gap is clinically significant given the limited efficacy of current immune checkpoint inhibitors (ICIs) in HCC therapy, partially attributable to inadequate biomarkers for patient stratification. Identifying molecules like BRAP that co-regulate tumor progression and immunosuppression could enable dual diagnostic/prognostic and therapeutic targeting.

This study integrated bioinformatics, clinical tissue analysis, and cytological experiments to assess BRAP expression in HCC and evaluate its correlation with clinicopathological characteristics and prognostic implications. Through lentiviral transfection, we validated BRAP's proliferative effects in vitro and in vivo, while RNA sequencing delineated its functional landscape. Combining multi-omics analyses with experimental validation, we further established BRAP's role in shaping the immunosuppressive tumor microenvironment. These findings provide mechanistic insights into BRAP-mediated oncogenesis and provide a rational basis for the development of BRAP-targeted therapeutic strategies in HCC.

Materials and Methods

Cell Culture and Human Tissues

The normal liver cell line L-02 and HCC cell line Huh7 were obtained from the American Type Culture Collection (ATCC, Manassas, USA). The HCC cell line HepG2 and human monocytes cell line THP-1 were sourced from the Cell Bank of the Chinese Academy of Sciences (Shanghai, China). L-02, Huh7 and HepG2 cells were incubated in Dulbecco's Modified Eagle's Medium (DMEM, Gibco, USA) supplemented with 10% fetal bovine serum (FBS; Gibco, USA). THP-1 cells were maintained in RPMI-1640 medium (Gibco, USA) with 10% FBS. All cell lines were incubated at 37°C in 5% CO2. The culture medium was changed every 2–3 days. Mycoplasma contamination testing confirmed all cell lines were negative. Paraffin-embedded tissue microarrays (HLivH060CD03 and HLivH180Su31) were purchased from Shanghai Outdo Biotechnology Company (Shanghai, China). The HLivH060CD03 array contained 2 normal liver tissues, 6 cirrhotic liver tissues, 17 tumor tissues, 17 adjacent non-tumor tissues, and 15 metastatic tumor tissues. The HLivH180Su31 array contained 97 tumor tissues and 83 adjacent non-tumor tissues.

Data Source

The clinical and molecular data for HCC patients (including mRNA expression and mutation data) were downloaded from the Cancer Genome Atlas (TCGA) Data Portal (https://tcga-data.nci.nih.gov/tcga/). Patients with insufficient or missing data were excluded from subsequent data processing. Ultimately, 371 patients from the TCGA cohort were evaluated; 321 patients only provided HCC tissues, and 50 patients also provided paired tissue samples (HCC tissues vs adjacent nontumor tissues). All HCC patients were classified into low- and high-BRAP expression groups according to the median BRAP expression value. Moreover, BRAP expression data and clinicopathological characteristics, including age, sex, pathological grade, tumor-node-metastasis (TNM) stage, and vascular invasion, were also extracted. The International Cancer Genome Consortium (ICGC) database (https://dcc.icgc.org/) includes 237 HCC samples in its LIRI-JP cohort.

Analysis of Diagnostic and Prognostic Value Using the Public Datasets

To explore whether the expression of the BRAP gene is related to the prognosis of HCC, we divided the cancer patients into high- and low-expression groups according to the expression value of BRAP and generated Kaplan-Meier curves. Overall survival (OS), progression-free survival (PFS), and disease-free survival (DFS) were used as endpoints. Time dependent receiver operating characteristic (ROC) curves were drawn to evaluate the prediction accuracy of the prognostic model.

Functional Enrichment Analysis Based on the TCGA Database

Functional annotation of the differentially expressed genes (DEGs) between the high- and low-BRAP expression groups was performed with the R package ClusterProfiler. Gene Ontology (GO) terms with P values < 0.05 were considered significantly enriched. The $\log_2$-fold change and P value calculated via the DESeq2 package were used as ranking metrics.

Analysis of the Tumor Microenvironment, Tumor Mutation Burden (TMB), and Immunotherapy Response via the TCGA Database

To explore whether the expression of BRAP is related to the tumor immune microenvironment, we first used the ESTIMATE algorithm to estimate the abundance of immune cells in HCC samples. The CIBERSORT algorithm was subsequently used to estimate the proportions of 23 types of infiltrating immune cells in the sample and compare these proportions between the high- and low-expression groups. Spearman correlation analysis was used to evaluate the correlation between infiltration and immune cell scores. In addition, the correlation between BRAP expression and immune checkpoint gene (ICG) levels was explored via correlation modules. To investigate the relationship between BRAP and tumor mutation burden (TMB), we analyzed the mutation annotation format (MAF) files of somatic variants and implemented the "maftools" R package, which provides various functions to perform the most commonly used analysis in cancer genomics and to create feature-rich customizable visualizations.[14] After comparing the TMB values between the high- and low-BRAP expression groups, we further analyzed the differences in gene mutation distribution and frequency between the high- and low-BRAP expression groups of samples.

Single-Cell RNA Sequencing (scRNA-Seq) Analysis of BRAP Expression

ScRNA-seq data from the GSE149614 dataset, obtained from the GEO database, were processed via the "Seurat" package. To ensure a high-quality scRNA-seq profile, three stringent quality control measures were applied to the raw gene-cell-barcode matrix for each cell: (1) cells must express more than 100 genes; (2) gene counts should range between 200 and 8000; and (3) mitochondrial gene expression should be less than 20%. The DoubletFinder package is used to eliminate double cells. Data normalization was performed using the "NormalizeData" function with a scaling factor of 10,000. The top 2000 highly variable genes were identified through the "Find Variable Feature" function. Dimensionality reduction was then performed using the RunPCA function, with the first 30 principal components selected for subsequent analyses. For batch effect correction in multi-sample data, the RunHarmony function of the Harmony package was used for data integration. BRAP expression was illustrated on the UMAP plot, whereas cluster annotation was performed on the basis of metadata from the original study.[15] All single-cell analyses were based on R language version 4.2.0.

Immunohistochemistry (IHC) and Scoring

To observe the expression of BRAP at the protein level, immunostaining was performed with paraffin-embedded tissue microarrays (HLivH060CD03 and HLivH180Su31). The paraffin sections were deparaffinized, rehydrated, and then subjected to high pressure for antigen retrieval in citric acid repair solution. Endogenous peroxidase activity was inactivated by incubation with 3% hydrogen peroxide, and nonspecific binding was blocked with 5% bovine serum. The slides were incubated with a primary rabbit anti-BRAP antibody (1:400, Abcam) at 4°C overnight. The negative control sections were stained as described but with the primary antibody omitted. BRAP protein expression was semiquantitatively estimated by adding the scores for the percentage of positive cells and the staining intensity. The percentage of positive cells was scored as follows: 0 for staining of ≤5%, 1 for staining of 6–25%, 2 for staining of 26–50%, 3 for staining of 51–75%, and 4 for staining of >75% of the cells examined. The staining intensity was scored as follows: 0, negative staining; 1, weak staining; 2, moderate staining; and 3, intense staining. The total staining score ranged from 0–12 and was used to categorize expression as low (IHC score<6) or high (IHC score≥6).[16] The scores were estimated independently by two experienced pathologists, and the average of the scores was considered the final assessment score.

Multiplex Immunofluorescence (mfIHC) Analysis

To characterize the immune landscape of HCC tissues, mfIHC was performed using Opal 7-Color IHC Detection Kits (NEL861001KT; Akoya Bioscience, USA) according to the manufacturer's instructions. First, the primary antibody was visualized via tyramide signal amplification linked to a specific fluorochrome from the mfIHC kit for each primary antibody, and the antibody panel was constructed on the basis of five antibody-stained sections. Next, the paraffin-embedded tissue microarray section was deparaffinized in xylene and rehydrated with a graded series of alcohols. Then, the sections were subjected to antigen retrieval with citrate acid buffer (pH 6.0)/Tris-EDTA buffer (pH 9.0) and blocked with blocking buffer.

The sections were incubated with the antigen-specific primary antibodies listed in Table S1. The multiplex-stained tissue microarray section was scanned using a Vectra® 3 multispectral microscope (Akoya Bioscience). All cube filters were used for each image capture (DAPI, Opal 520, Opal 570, Opal 650, Opal 480, and Opal 780). The incorporated saturation protection feature was set at an exposure time of 250 ms. These data were analyzed via InForm 2.6 software.

Quantitative Real-Time Polymerase Chain Reaction (qRT–PCR)

Total RNA was extracted from the cell lines using TRIzol reagent (Thermo Fisher Scientific, USA) according to the manufacturer's instructions. Total RNA (1 μg) was reverse transcribed using the PrimeScript RT Reagent Kit (Takara, Dalian, China) according to the manufacturer's instructions. cDNA was subsequently amplified via qRT–PCR on an Applied Biosystems 7500 Real-Time PCR system (Applied Biosystems, USA) with SYBR Premix DimerEraser (Takara, Dalian, China). The relative expression of BRAP was calculated via the $2^{-\Delta\Delta Ct}$ method with GAPDH as the control for normalization. The primers used are described in Table S2.

Western Blotting

The cells were lysed in RIPA buffer containing a protease/phosphatase inhibitor cocktail (Beyotime, China). The Pierce BCA Protein Assay Kit (Thermo Fisher Scientific, MA, USA) was used to determine the protein concentrations. Proteins were then separated on a 10–12% separation gel and transferred onto PVDF membranes (Millipore, MA, USA). A 5% milk powder mixture was added to block nonspecific binding. The membranes were incubated overnight at 4°C with the primary antibodies listed in Table S1 and then with HRP-conjugated goat anti-mouse or -rabbit secondary antibodies (1:5000, Cell Signaling Technology) at room temperature for 2 h. An enhanced chemiluminescence kit (ECL; Millipore, USA) was subsequently used for detection of the immunoreactive bands.

Lentiviral Packaging

ShRNAs targeting BRAP were synthesized, and the sequences are shown in Additional file 1: Table S3. The shRNA-BRAP or shRNA-NC was inserted into the pLKO.1 vector and cotransfected into 293T cells with the packaging plasmids psPAX2 and pMD2G (Addgene) using the Lipofectamine 3000 Transfection Kit (Thermo Fisher Scientific, MA, USA). After transfection, the cell supernatants were harvested and used to transduce Huh7 and HepG2 cells; the stably transduced cells were selected with puromycin (3 μg/mL) for 1 month.

CCK-8 Assay

Cell proliferation was assessed via CCK-8 assay. The cells were seeded at an initial density of 5×10^4 cells/well in 96-well plates. After adhesion, the cells were cultured in DMEM at 37°C for 0, 24, 48, or 72 h. Then, 10 μL of CCK-8 reagent (Beyotime, Shanghai, China) was added to the wells at each time point, and the mixture was further incubated for 2 h. The absorbance was measured at 450 nm via a microplate reader (Bioteck, USA). Five wells were prepared for each group for the CCK-8 assay.

Colony Formation Assay

The cells were seeded at a density of 1000 cells/well with DMEM at 37°C in 6-well plates. At 14 days, the colonies were washed twice with PBS, fixed with paraformaldehyde for 30 min and stained with 0.1% crystal violet for 30 min. The cell colonies were imaged, and the number of colonies was counted for statistical analysis. All experiments were independently repeated at least three times under identical conditions.

5-Ethynyl-2′-Deoxyuridine Assay (EdU) Assay

The cells were seeded on coverslips and incubated with DMEM for 48 h. The cells were treated with 50 mM EdU for 4 h at 37°C and stained with an anti-EdU antibody (RiboBio, Guangzhou, China) according to the manufacturer's instructions. The images were observed under a fluorescence microscope. The percentage of EdU-positive cells was calculated from five random fields per well. Approximately 200 cells were observed in each well. The EdU-labeled (red) and unlabeled (blue) cells were counted. The EdU labeling index (%) was calculated as labeled (red) cells/ [labeled (red) cells+unlabeled (blue) cells] ×100%. Three independent experiments were performed.

Flow Cytometric Analysis

The cells in the logarithmic growth phase were seeded at an initial density of 1×10^5 cells and cultured overnight, after which the cells were harvested. For cell cycle analysis, the cells were rinsed in precooled PBS, followed by fixation with 75% alcohol overnight at 4°C. Then, the cells were digested with 1% RNase A (Beyotime, Shanghai, China) and stained with 1 mg/mL propidium iodide (PI) (Beyotime, Shanghai, China) for 30 min in the dark. Cell cycle distraction was assessed using a flow cytometer (Beckman, CytoFLEX, USA). The results were recorded and analyzed via C Flow Plus and Mod Fit LT 3.3 software.

THP-1 monocytes were differentiated into M0 macrophages using 100 ng/mL phorbol 12-myristate 13-acetate (PMA) for 48 h. Subsequently, M0 macrophages and HepG2 cells were co-cultured for 7 days. On day 7 of co-culture, adherent macrophages cells were collected. These adherent cells were first washed with PBS, then detached using cell dissociation buffer (Thermo Fisher Scientific, MA, USA). The detached cells were combined with the previously collected culture medium for subsequent washing steps. Next, the suspended cell mixture was centrifuged and washed twice with PBS supplemented with 0.5% BSA and 2 mM EDTA, followed by cell counting. For flow cytometric analysis, these cells were incubated with fluorophore-conjugated primary antibodies: anti-CD206 (FITC-conjugated) and anti-iNOS (PE-Cy3-conjugated). Incubation was performed for 45 min at 4°C in the dark to prevent fluorophore photobleaching. Fluorescence signals were detected and analyzed using C Flow Plus software and Mod Fit LT 3.3 software, respectively. For macrophage polarization experiments: M1 polarization was induced by stimulating M0 macrophages with IFN-γ (20 ng/mL) and LPS (20 ng/mL) for 48 h. M2 polarization was induced by treating M0 macrophages with IL-4 (20 ng/mL) for 48 h.[17]

Animal Experiments

All animal experiments complied with the ARRIVE guidelines and were approved by the Animal Research Ethics Committee of Zhengzhou University (Zhengzhou, China; ZZU-LAC20220909). Four-week-old athymic BALB/c female nude mice (nu/nu) were purchased from Shanghai Model Organisms (Shanghai, China). Approximately 5×10^6 HepG2 cells with sh-BRAP-#2, sh-CTRL, or LV-BRAP or LV-CTRL were suspended in 100 μL of PBS and subcutaneously injected into the left flank of each mouse. Each experimental group contained five mice. The tumor volume was monitored every 3 days. Tumor size was calculated on the basis of Vernier caliper measurements of the length and width of the lesions using the following formula: $0.5\times\text{length}\times\text{width}^2$. After 21 days, the mice were sacrificed for cervical dislocation after carbon dioxide anesthesia, and the tumors were removed for further histological examination. Freshly dissected tumors were fixed to prepare formalin-fixed paraffin embedded (FFPE) samples. The resulting sections were subjected to IHC staining against specific antigens.

Statistical Analysis

SPSS 23.0 software (SPSS Inc., Chicago, USA) and GraphPad Prism 7.0 software (GraphPad Software Inc., Chicago, USA) were used for statistical analysis. The data are presented as the mean±SD, and differences between two groups were assessed via Student's *t* test, whereas differences among more than two groups were assessed via one-way ANOVA, followed by Tukey's post hoc test for multiple comparisons. The associations between BRAP expression and clinical data were analyzed via Pearson's chi-square test. The prognostic value was estimated by comparing groups via the Kaplan-Meier method with the Log rank test. *P* values for descriptive data were generated for the variables. For univariate and multivariate analyses, the Cox proportional-hazards model was utilized to explore the impact of various variables on survival outcomes. Each experiment was repeated three times. Statistical significance was considered at $P<0.05$.

Results

HCC Patients with Elevated BRAP Levels Have Poor Prognosis

To elucidate the expression patterns of BRAP in HCC, we first performed IHC analysis on a paraffin-embedded liver tissue microarray (TMA) comprising normal liver tissues, cirrhotic tissues, paracancerous tissues, and HCC tissues. Our findings revealed that BRAP was predominantly localized to the cytoplasm. The IHC images and corresponding scores indicated that BRAP expression in HCC tissues was significantly higher than normal liver tissues, cirrhotic tissues, and paracancerous tissues (Figure 1A and B and Figure S1A-B). To exclude the effects of individual patient variations, we

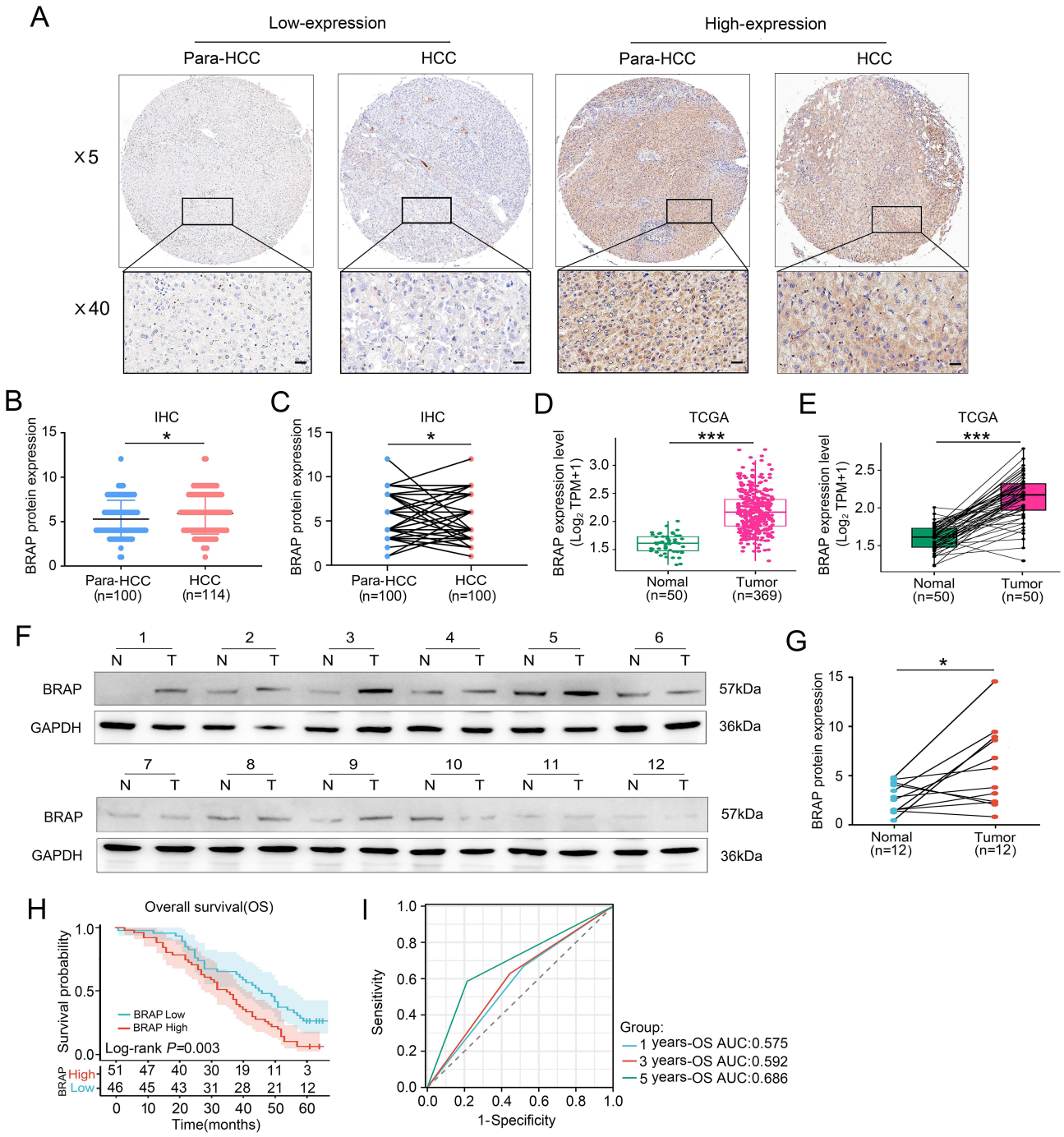

Figure 1 Analysis of the correlation of BRAP expression with HCC prognosis. (**A**) Representative immunohistochemistry (IHC) images depicting BRAP expression in paracancerous tissues and HCC tissues (scale bar=20 μm). (**B** and **C**) Quantitative assessment of BRAP expression levels in paracancerous tissues and HCC tissues. (**D**) Comparison of BRAP expression levels between nontumor tissues and HCC tissues derived from the TCGA. (**E**) Paired analysis of BRAP expression in nontumor tissues versus HCC tissues from the TCGA. (**F** and **G**) Western blotting images (left) and quantification (right) of BRAP expression levels in 12 pairs of paracancerous tissues and HCC tissues. (**H**) Kaplan-Meier survival analysis comparing OS between the high and low BRAP expression groups. (**I**) ROC curve illustrating the predictive value of BRAP expression for overall survival at 1, 3, and 5 years. The data are presented as the mean ± SD. *$P < 0.05$; ***$P < 0.001$.

analyzed BRAP expression in HCC tissues versus matched paracancerous tissues. Consistent with our initial observations, BRAP expression was significantly elevated in HCC tissues compared to paired paracancerous tissues (Figure 1C). These findings were validated by analysis of TCGA-LIHC data (Figure 1D and E). Furthermore, Western blotting of 12 pairs of freshly collected HCC and paracancerous tissue samples revealed a general increase in BRAP expression in HCC samples (Figure 1F and G). Our in-depth analysis further revealed a significant correlation between high BRAP protein

https://doi.org/10.2147/JHC.S547105

expression and advanced pathological grade, as well as poor OS (Table 1 and Figure 1H). Subsequent multivariate Cox regression analyses, incorporating risk score and clinical characteristics, identified BRAP as an independent prognosticator for OS (Table S4). Additionally, time-dependent ROC curves were generated to evaluate the predictive value of

Table 1 Clinicalpathological Features of Patients and Correlation with BRAP Protein Expression in HCC

Characteristics n (%)	Total n= 97	BRAP-Low n=46	BRAP-High n=51	χ^2	*P*
Age (years)				0.670	0.413
≤60	70 (72.2%)	35 (36.1%)	35 (36.1%)		
>60	27 (27.8%)	11 (11.3%)	16 (16.5%)		
Gender				5.240	0.022
Male	84 (86.6%)	36 (37.1%)	48 (49.5%)		
Female	13 (13.4%)	10 (10.3%)	3 (3.1%)		
Pathology grade				6.939	0.031
G1	4 (4.1%)	3 (3.1%)	1 (1.0%)		
G2	46 (47.4%)	27 (27.8%)	19 (19.6%)		
G3	47 (48.5%)	16 (16.5%)	31 (32.0%)		
HBsAg				0.078	0.780
Negative	33 (34.0%)	15 (15.5%)	18 (18.6%)		
Positive	64 (66.0%)	31 (32%)	33 (34%)		
AFP (ug/L)				0.032	0.857
≤400	73 (75.3%)	35 (36.1%)	38 (39.2%)		
>400	24 (24.7%)	11 (11.3%)	13 (13.4%)		
Tumor size (cm)				0.958	0.328
≤5	43 (44.3%)	18 (18.6%)	25 (25.8%)		
>5	54 (55.7%)	28 (28.9%)	26 (26.8%)		
Liver cirrhosis				3.790	0.052
No	35 (36.1%)	12 (12.4%)	23 (23.7%)		
Yes	62 (63.9%)	34 (35.1%)	28 (28.9%)		
TNM stage				3.284	0.350
Stage I	17 (17.5%)	9 (9.3%)	8 (8.2%)		
Stage II	19 (19.6%)	8 (8.2%)	11 (11.3%)		
Stage III	58 (59.8%)	29 (29.9%)	29 (29.9%)		
Stage IV	3 (3.1%)	0 (0%)	3 (3.1%)		
PVTT				4.433	0.035
No	83 (85.6%)	43 (44.3%)	40 (41.2%)		
Yes	14 (14.4%)	3 (3.1%)	11 (11.3%)		

Abbreviations: AFP, alpha fetoprotein; HBV, hepatitis B virus; PVTT, portal vein tumor thrombus.

BRAP expression for OS in HCC patients. As shown in Figure 1I, the area under the curve (AUC) values for BRAP expression at 1, 3, and 5 years were 0.575, 0.592, and 0.686, respectively.

To further confirm the diagnostic and prognostic significance of BRAP mRNA levels in HCC, we assessed their relationship with various clinicopathological parameters using the TCGA-LIHC dataset. BRAP mRNA expression was notably higher in advanced TNM stages (Figure S1C and Table S5). Consistent with previous findings, patients with high BRAP levels exhibited poorer OS, disease-free survival (DFS), and progression-free survival (PFS) compared than those with low BRAP levels (Figure S1D). ROC curve analysis also confirmed that BRAP expression significantly contributed to predicting prognosis in HCC patients (Figure S1E). To validate the robustness of these observations, we further evaluated BRAP's performance in the ICGC-LIRI-JP cohort. BRAP expression in HCC tissues was significantly higher than in normal liver tissues (Figure S1F). Patients in this cohort were stratified into high-and low-BRAP expression groups. Consistent with TCGA cohort findings, the high-BRAP group had significantly poorer survival outcomes. Kaplan-Meier survival analysis further confirmed that high BRAP expression was significantly correlated with reduced OS in HCC patients ($P<0.001$) (Figure S1G). Additionally, the AUC values for predicting 1-, 3-, and 5-year OS were 0.597, 0.641, and 0.687, respectively (Figure S1H). Collectively, these findings indicate that BRAP is upregulated in HCC and correlates with advanced pathological grades and poor prognosis.

BRAP Promotes HCC Cell Proliferation in vitro

To elucidate the pivotal role of BRAP in regulating the malignant process of HCC, we embarked on an initial assessment of its expression patterns in vitro across diverse cell lines. Our research revealed that both BRAP mRNA and protein levels were significantly elevated in two HCC cell lines (Huh7 and HepG2) compared with those in the normal liver cell line L-02 (Figure 2A). Subsequently, stable knockdown of BRAP was achieved in Huh7 and HepG2 cells via the use of two distinct shRNAs (sh-BRAP-#1/2). In parallel, we established HepG2 cells with a stable upregulation of BRAP through transfection with LV-BRAP lentivirus. The efficacy of both the knockdown and upregulation strategies was validated via qRT-PCR and Western blotting analyses, respectively. Compared with the control shRNA (sh-CTRL), both

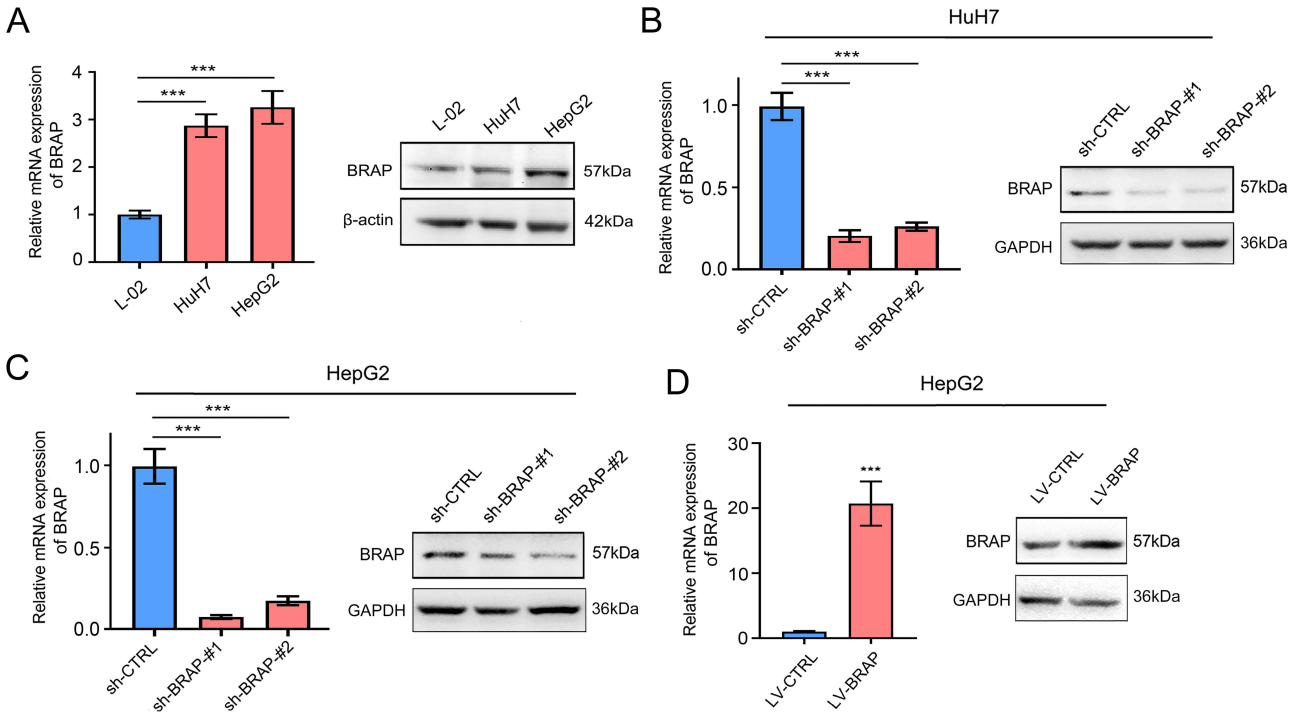

Figure 2 BRAP expression levels in HCC cell lines. (**A**) The mRNA and protein levels of BRAP were assessed in a normal liver cell line (L-02) and HCC cell lines (Huh7 and HepG2) via qRT–PCR and Western blotting analysis. (**B** and **C**) qRT–PCR and Western blotting analyses confirmed the efficiency of BRAP knockdown in Huh7 and HepG2 cells transduced with sh-BRAP or sh-CTRL. (**D**) The upregulation of BRAP expression in HepG2 cells transduced with LV-BRAP or LV-CTRLwas validated via qRT–PCR and Western blotting. Data are represented as mean ± SD and representative of three independent experiments. ***$P < 0.001$.

https://doi.org/10.2147/JHC.S547105

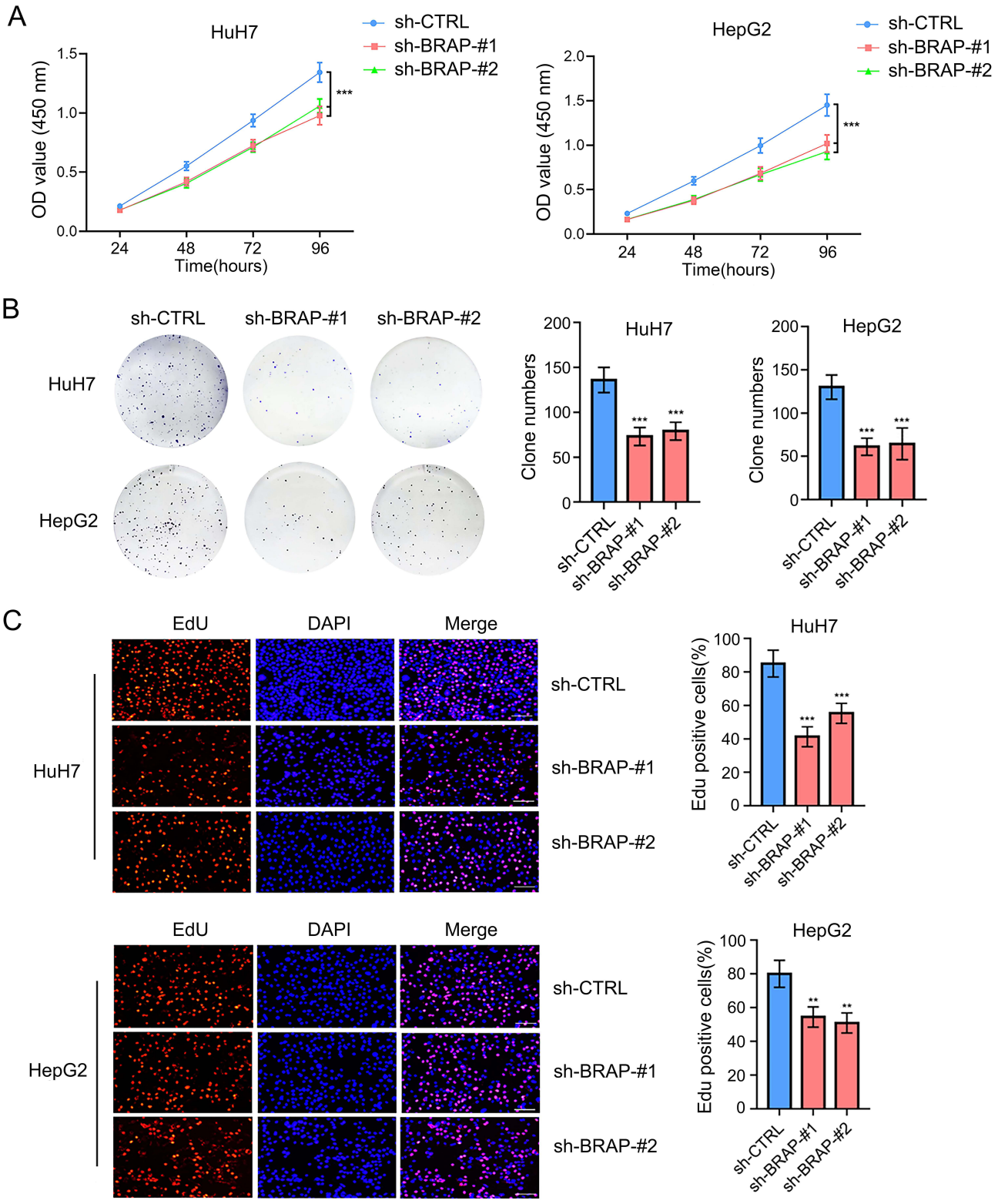

Figure 3 Knockdown of BRAP inhibits malignant proliferation in HCC. (**A**) CCK-8 assay was used to assess the viability of Huh7 and HepG2 cells. (**B** and **C**) Assessment of Huh7 and HepG2 cell proliferation was conducted via colony formation and EdU assays (scale bar=50 μm). Data are represented as mean ± SD and representative of three independent experiments. $^{**}P < 0.01$; $^{***}P < 0.001$.

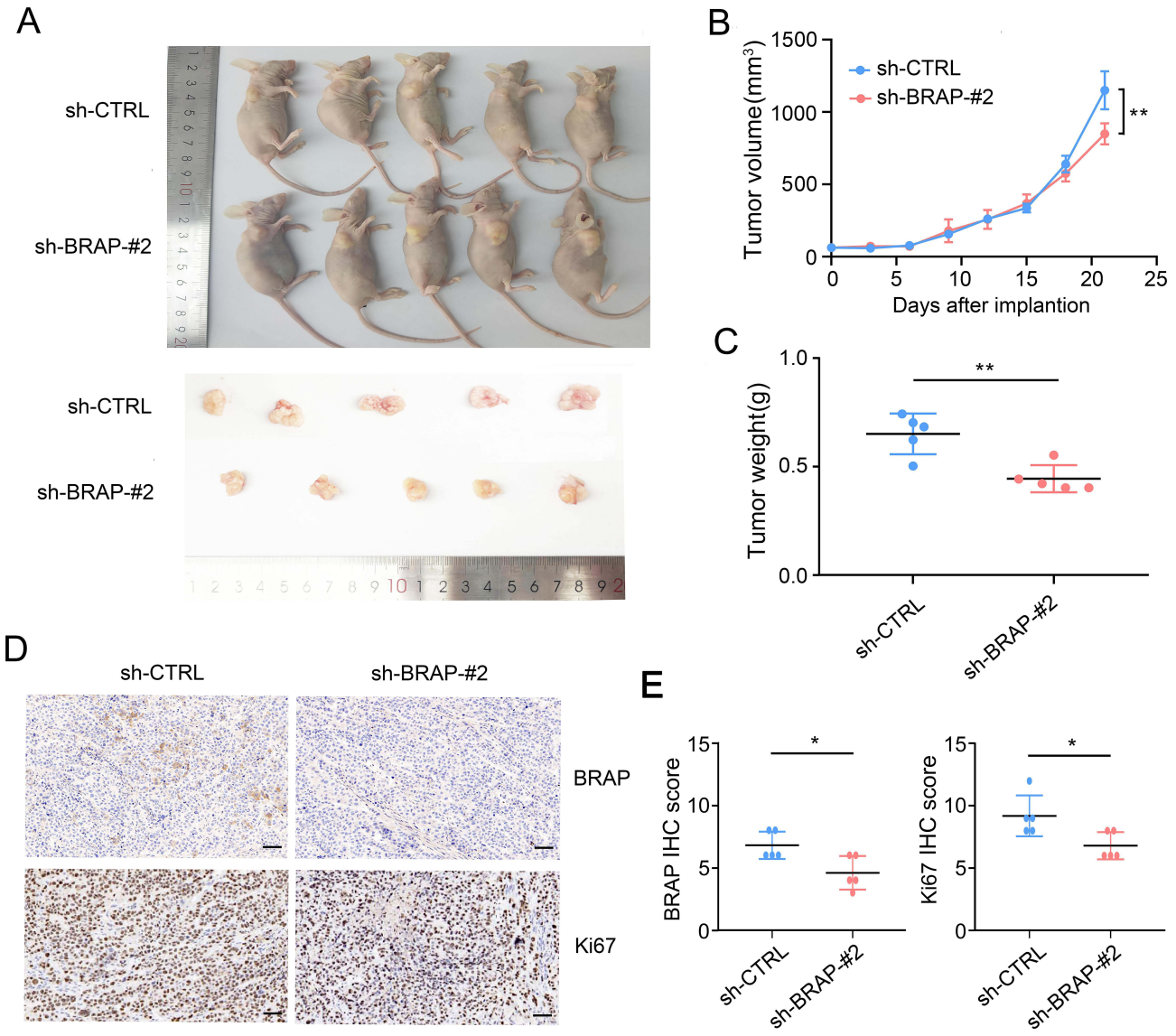

Figure 4 Silencing BRAP inhibits the growth of HCC tumors in vivo. (**A**) Images depicting the transplantation of HepG2 cells into nude mice to establish a tumor growth model. (**B** and **C**) The tumor growth curves and weights were compared between nude mouse xenografts transduced with sh-BRAP or sh-CTRL HepG2 cells. (**D** and **E**) IHC staining and quantitative analysis of the expression levels of BRAP and Ki67 in the sh-BRAP and sh-CTRL groups (scale bar=20 μm). Data are represented as mean ± SD. **P* ≤0.05; ***P* < 0.01.

sh-BRAP-#1 and sh-BRAP-#2 effectively reduced BRAP mRNA and protein levels in Huh7 and HepG2 cells. Additionally, BRAP expression was significantly increased in HepG2 cells following LV-BRAP transfection (Figure 2B–D). After confirming successful knockdown of BRAP, CCK-8 assays were performed and indicated that downregulation of BRAP markedly decreased the percentage of viable Huh7 and HepG2 cells in vitro (Figure 3A). Consistently, colony formation and EdU assays demonstrated that the knockdown of BRAP substantially decreased the proliferation rates of both Huh7 and HepG2 cells when compared to their respective control groups (Figure 3B and C). Taken together, these results show that BRAP promotes cell proliferation in HCC.

BRAP Knockdown Inhibits the Growth of HCC Tumors in vivo

To further validate the effect of BRAP on tumor growth in vivo, ten nude mice were randomly assigned to two groups. HepG2 cells from the control group (sh-CTRL) and the experimental group (sh-BRAP-#2) were injected into the subcutaneous tissue of the left flank of each mouse, respectively. The tumor growth was meticulously monitored over time. After three weeks, the

https://doi.org/10.2147/JHC.S547105

nude mice were euthanized in accordance with ethical guidelines, and the subcutaneously implanted tumors were surgically excised. As shown in Figure 4A, the shRNA-mediated knockdown of BRAP resulted in notable decrease in tumorigenicity when compared to the control group. The tumors in the sh-BRAP-#2 group exhibited significantly smaller volumes and lower weights than those in the control group, as illustrated in Figure 4B and C. Furthermore, IHC analysis of tumor tissues revealed that BRAP knockdown markedly decreased expression of Ki67, a well-established marker for cell proliferation (Figure 4D and E). Conversely, when HepG2 cells were overexpressing BRAP (LV-BRAP), a distinct pattern emerged. Compared to the control cells (LV-CTRL), the LV-BRAP cells demonstrated accelerated tumor growth, evidenced by substantial increases in both tumor volume and weight. Additionally, there was a pronounced elevation in Ki67 expression within the LV-BRAP group (Figure S2A-E). Together, these results show that loss of BRAP inhibit the growth of HCC tumors in vivo.

Transcriptomic Profiling of Differentially Expressed Genes (DEGs) After BRAP Knockdown and Analysis of Related Biological Processes

To elucidate the biological functions of BRAP, we initially utilized our RNA-seq data to screen for DEGs in HepG2 cells transduced with sh-CTRL, sh-BRAP-#1, or sh-BRAP-#2. As shown in Figure 5A and B, a total of 1567 DEGs were

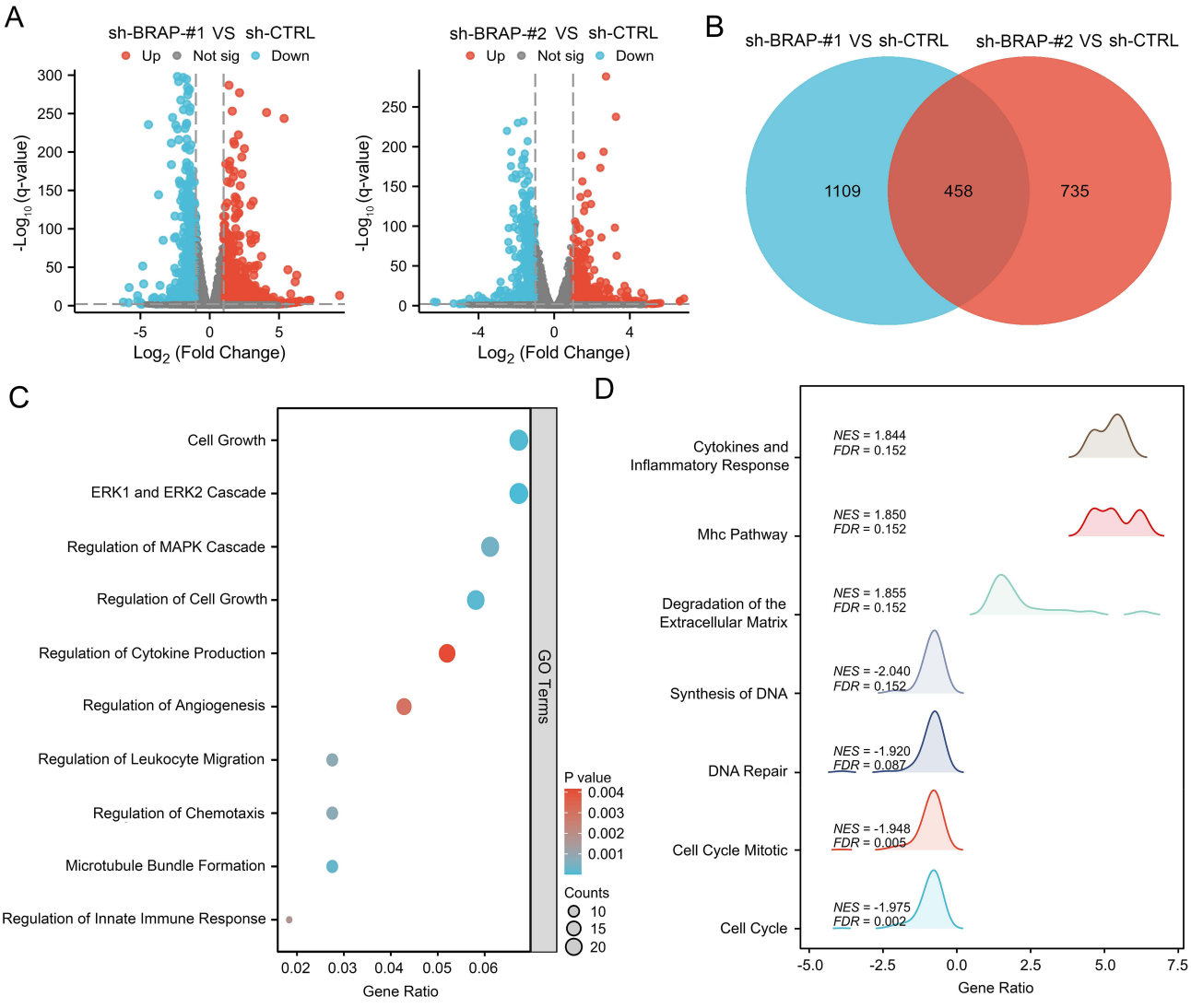

Figure 5 Functional enrichment analysis of BRAP in HCC on the basis of the RNA-seq dataset. (**A**) Volcano plots illustrating the distribution of DEGs between sh-CTRL and sh-BRAP-#1, as well as between sh-CTRL and sh-BRAP-#2 derived from RNA-seq data. (**B**) The coexpression of DEGs is represented via a Venn diagram. (**C** and **D**) Bubble plot and ridgeline plot displaying the GO and GSEA results for the overlapping DEGs.

identified between the sh-CTRL and sh-BRAP-#1 groups, whereas 1193 DEGs were found between the sh-CTRL and sh-BRAP-#2 groups. Among these, 458 overlapping DEGs were selected for further analysis. We subsequently conducted GO functional enrichment analysis of these 458 overlapping DEGs. The results indicated that the overlapping DEGs were enriched in biological processes such as cell growth, cytokine production, leukocyte migration, and MAPK signaling pathways (Figure 5C). Furthermore, gene set enrichment analysis (GSEA) confirmed that BRAP significantly influenced cytokine activity and inflammatory responses as well as DNA synthesis and cell cycle pathways (Figure 5D). Finally, we validated the biological processes associated with BRAP with the TCGA-LIHC dataset to identify DEGs among HCC tissues exhibiting low versus high BRAP expression compared with normal liver tissues (Figure S3A-B). We performed GO analysis on the overlapping DEGs across these three groups; the top 20 enriched terms were identified (Figure S3C). Many of the most highly enriched biological processes were closely related to cell cycle regulation, including chromosome segregation, organelle fission, nuclear division, and DNA replication pathways.

Downregulation of BRAP Suppresses the Proliferation of HCC Cells by Inducing Cell Cycle Arrest

Previous functional enrichment analysis indicated that BRAP significantly influences the regulation of the cell cycle. To validate whether shRNA-mediated BRAP knockdown inhibits HCC cell proliferation by inducing cell cycle arrest, we performed flow cytometric analysis. In HepG2 cells, BRAP silencing significantly increased the proportion of cells in the G0/G1 phase, while reducing cell populations in both the G2/M and S phases. Notably, in Huh7 cells, BRAP knockdown exerted a distinct effect: it significantly elevated the G2/M phase fraction, with a concurrent reduction in S phase cells (Figure 6A). To rule out shRNA off-target effects, we designed two BRAP-targeting siRNAs (si-BRAP-#1/#2) and conducted rescue experiments. qRT-PCR and Western blotting analyses confirmed that both siRNAs effectively downregulated BRAP expression at the mRNA and protein levels in HepG2 cells (Figure S4A-B). Consistently, these siRNAs suppressed HepG2 cell proliferation and induced G1/S phase arrest. Furthermore, transfecting si-BRAP-#1 into HepG2 cells with stable BRAP overexpression (LV-BRAP) reversed the excessive proliferation phenotype driven by BRAP overexpression. For the cell cycle, the G0/G1 phase arrest rate was reduced in the LV-BRAP+si-BRAP group compared to the LV-BRAP group (Figure S4C-E).

We subsequently conducted Western blotting analyses to detect the expression levels of cell cycle-related proteins. As shown in Figure 6B, BRAP knockdown significantly suppressed Cyclin B1 and CDK1 expression in Huh7 cells; however, no substantial inhibition of cyclin D1 or CDK4 expression was detected. In contrast to that in Huh7 cells, downregulation of BRAP resulted in increased p21 expression but decreased Cyclin D1 and CDK4 levels in HepG2 cells. Conversely, opposite effects were observed following BRAP overexpression. These Western blotting results are consistent with those of our cell cycle flow cytometry analysis. Notably, the initiation of mitosis at the G2/M checkpoint requires the activation of cyclin B1/CDK1 complexes.[18] Furthermore, differences in the regulation of the cell cycle by BRAP suggest that variations in p53 mutation status—specifically, the p53Y220C mutation present in Huh7 cells versus the wild-type p53 (WT-p53) found in HepG2 cells—may contribute to these discrepancies. However, much more work needs to be carried out. Collectively, knockdown of BRAP inhibits the proliferation of HCC cells by inducing cell cycle arrest.

BRAP Promotes the Proliferation of HCC Cells by Activating the MAPK/ERK Signaling Pathway

The MAPK/ERK signaling pathway, a highly conserved signaling cascade, plays a crucial role in tumorigenesis.[19] An in-depth analysis of our RNA-Seq data through GSEA revealed a significantly enrichment of BRAP-associated genes within the MAPK/ERK signaling pathway (Figure 7A and B). Upon silencing the expression of BRAP in HCC cells, we observed a notable decrease in the phosphorylation levels of ERK1/2, MEK1, and Raf1. Conversely, the upregulation of BRAP led to a marked activation of the Raf1-MEK1-ERK1/2 pathway, as evidenced by Western blotting analysis (Figure 7C). To further elucidate the functional implications of this pathway, we assessed the potential effects of the ERK1/2 inhibitor PD98059 on cell cycle arrest. As shown in Figure 7D, PD98059 effectively inhibited the progression of

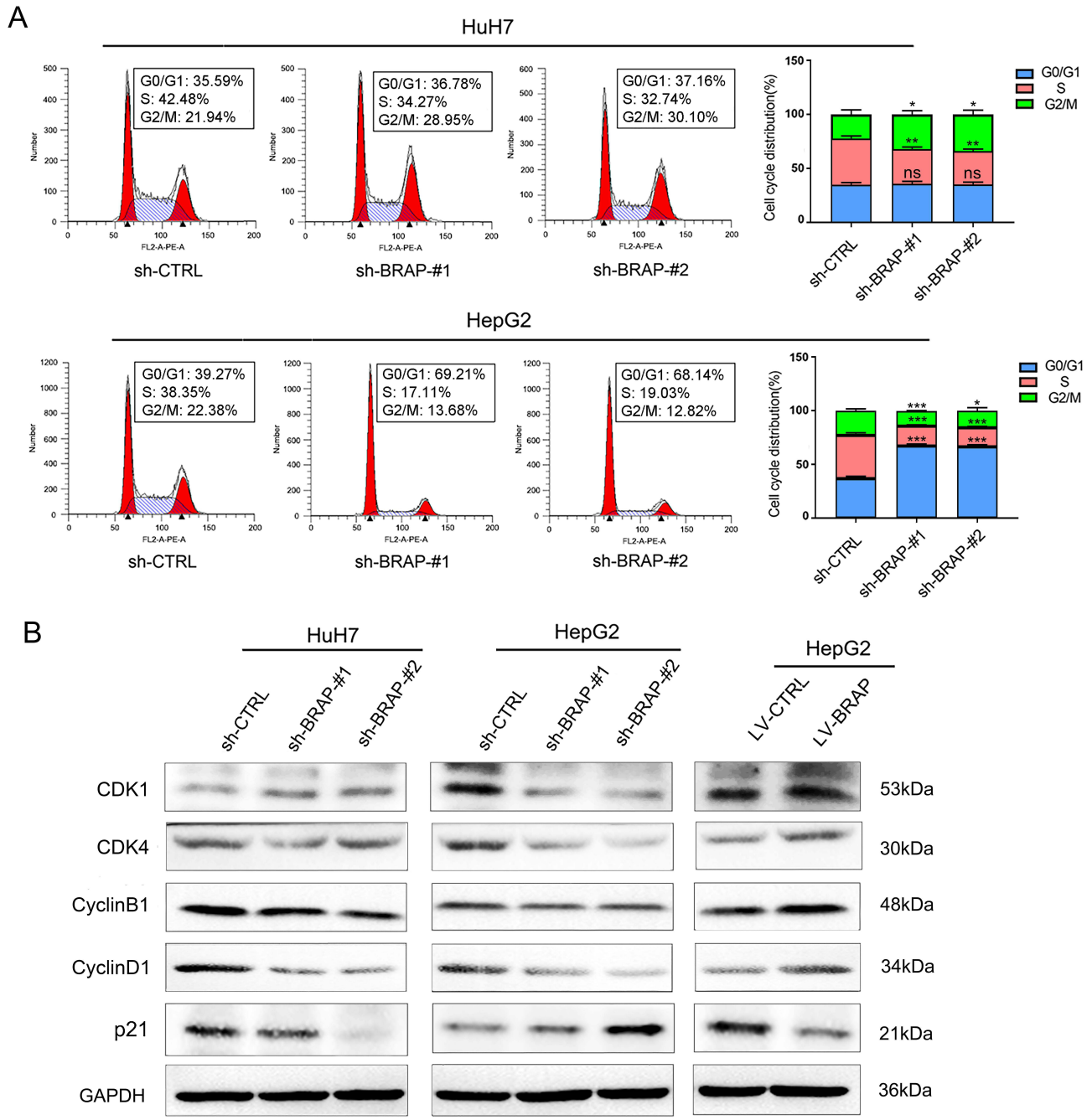

Figure 6 Silencing BRAP induces cell cycle arrest in HCC cells. (**A**) Representative image (left) and quantification (right) of the results of the cell cycle phase assay in Huh7 and HepG2 cells transduced with sh-BRAP or sh-CTRL. (**B**) Western blotting analysis showing the expression of cell cycle-related proteins in the low- and high-BRAP expression groups. Data are represented as mean ± SD and representative of three independent experiments. ns: *P>0.05;*P* ≤0.05; ***P* < 0.01; ****P* < 0.001.

the cell cycle in Huh7 cells. Moreover, the deletion of BRAP synergistically enhanced this inhibitory effect. Collectively, our findings provide compelling evidence that the MAPK/ERK signaling pathway is intricately involved in BRAP-mediated proliferation of HCC cells.

BRAP Expression Patterns and Implications in the HCC Tumor Microenvironment

The tumor microenvironment inherently influences the development and prognosis of HCC.[20,21] To investigate the distribution of BRAP within the tumor microenvironment of HCC, we employed scRNA-seq data from the GSE149614 dataset, which includes data on 10 HCC patient samples with primary and/or metastatic tumors representing various

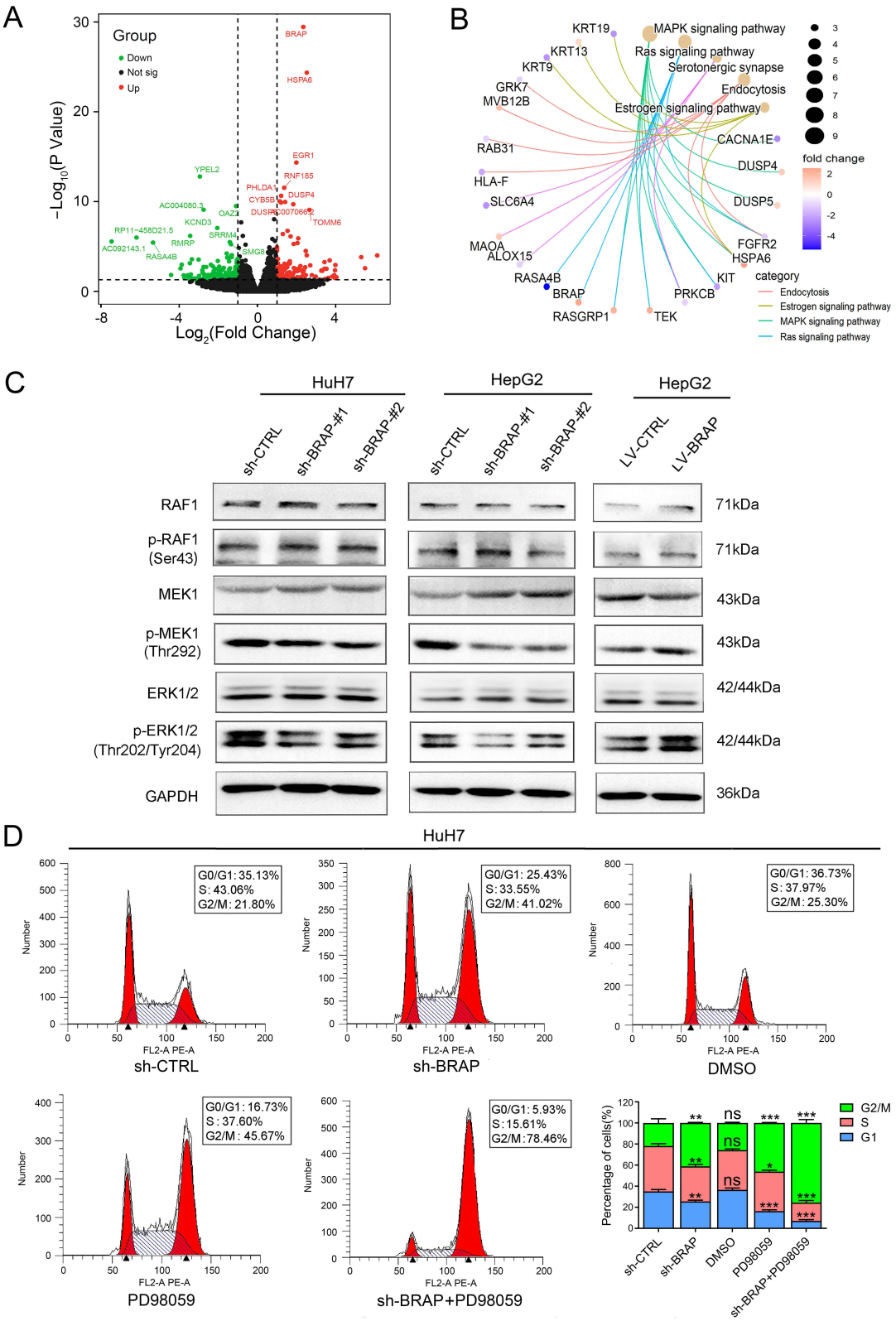

Figure 7 BRAP promotes HCC cell proliferation by activating the MAPK/ERK signaling pathway. (**A**) Volcano plot illustrating the distribution of DEGs between LV-control and LV-BRAP HepG2 cells. (**B**) Circos plot showing BRAP expression in relation to the activation of the MAPK/ERK signaling pathway. (**C**) Western blotting analysis confirming that BRAP induces activation of the MAPK/ERK signaling pathway in HCC cells. (**D**) Representative images (left) and quantification (right) of the results of the cell cycle phase assay in sh-CTRL, sh-BRAP, sh-CTRL+DMSO (DMSO), sh-CTRL+PD98059 (PD98059), sh-BRAP+PD98059 group, and the specified stable HuH7 cell lines treated with 10μM ERK1/2 inhibitor PD98059 for 24h. Data are represented as mean ± SD and representative of three independent experiments. ns: $P>0.05$;*$P \leq 0.05$; **$P < 0.01$; ***$P < 0.001$.

https://doi.org/10.2147/JHC.S547105

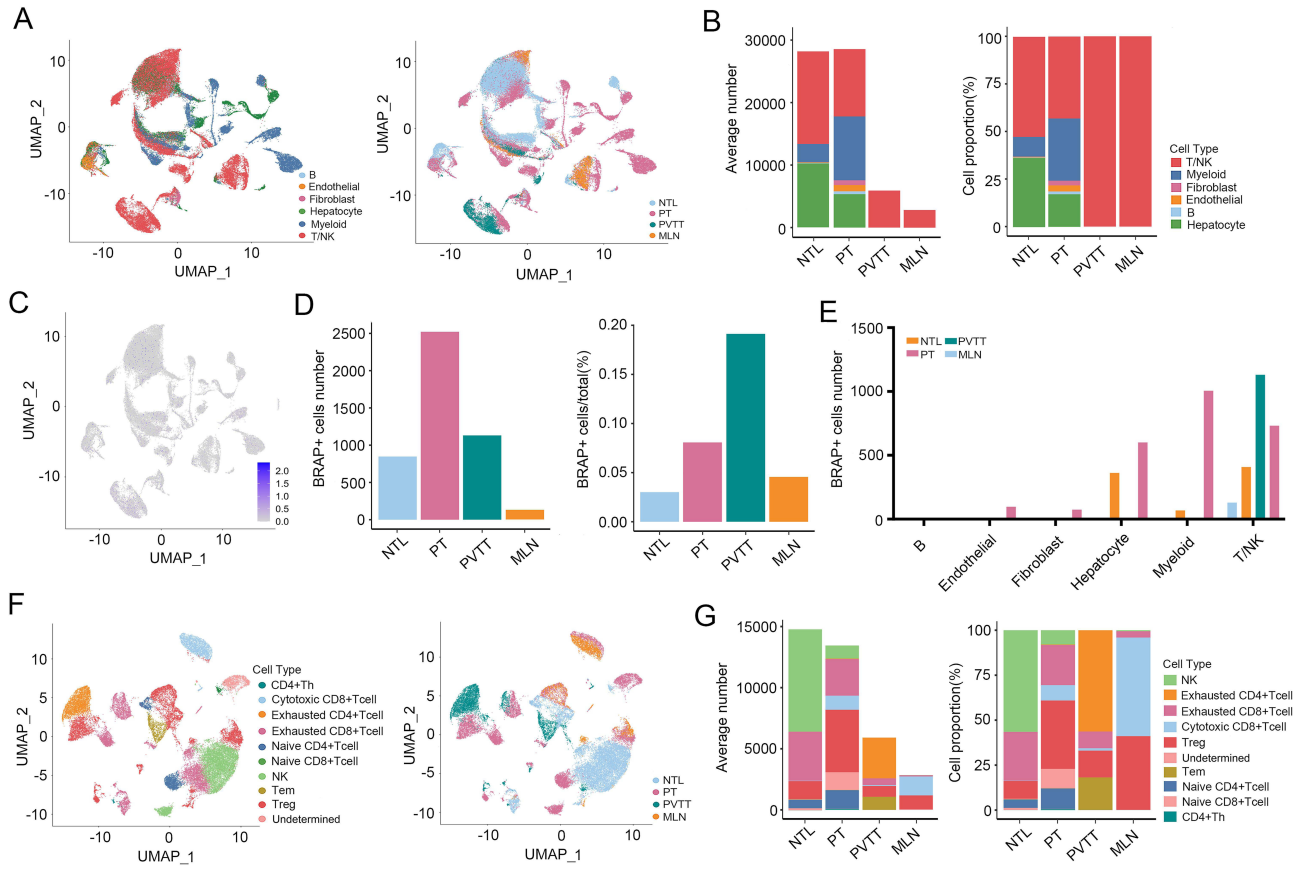

Figure 8 Single-cell sequencing analysis reveals the distribution pattern of BRAP-positive cells in HCC. (**A**) UMAP plot visualization of 71,915 cells categorized by diverse cell types and different origins from 10 HCC patients. (**B**) Average cell counts and relative proportions of major cell types across each tissue type. (**C**) Relative expression levels of BRAP among 71,915 cells visualized via a UMAP plot. (**D**) The number (left) and proportion (right) of BRAP-expressing cells across various tissue types. (**E**) BRAP expression levels in different cell types and tissue contexts. (**F**) UMAP plot depicting T/NK cell clusters. (**G**) Average cell counts and relative proportions of T/NK cell subsets within each group.

TNM stages. The transcriptomes of individual cells were analyzed across four relevant tissue types: non-tumor liver (NTL), primary tumor (PT), portal vein tumor thrombus (PVTT), and metastatic lymph node (MLN) tissues. Following quality control and the removal of the double cells, a total of 68,114 single cells were selected for further analysis. The results indicated that BRAP expression was detected in multiple cell types, with hepatic epithelial cells and T/NK cells exhibiting the highest abundance (Figure 8A and B). Among the 4628 cells expressing BRAP, the majority originated from tumor tissues (Figure 8C and D). T/NK cells account for the largest proportion compared to other types of cells among the four tissue types. Interestingly, BRAP-positive cells are mainly concentrated in T/NK cells, especially PVTT presented the highest proportion and number of BRAP-expressing cells (Figure 8E). This indicates that compared with bulk data, single-cell data can better reflect the changes in gene expression levels among different types of cells. Indeed, the elevated BRAP expression observed in PT coincided with a greater proportion of BRAP-expressing cells than in NTL-expressing cells. Given the predominant BRAP expression in T/NK cells within the NTL, we further investigated its potential functional impact on these cell types within the tumor environment. Reclustering of 3660 BRAP-expressing T/NK cells yielded ten subclusters identified as NK cells, naive CD4+ T cells, naive CD8+ T cells, CD4+T helper cells, cytotoxic CD8+ T cells, exhausted CD4+ T cells, exhausted CD8+ T cells, and regulatory T cells (Tregs) (Figure 8F). Tumor tissues presented decreased infiltration of NK cells and concomitant increased infiltration of naive CD4+ T cells, naive CD8+ T cells and Tregs (Figure 8G). These findings suggest a potential role for BRAP in regulating the activation and function of T/NK cells, but further investigation is needed.

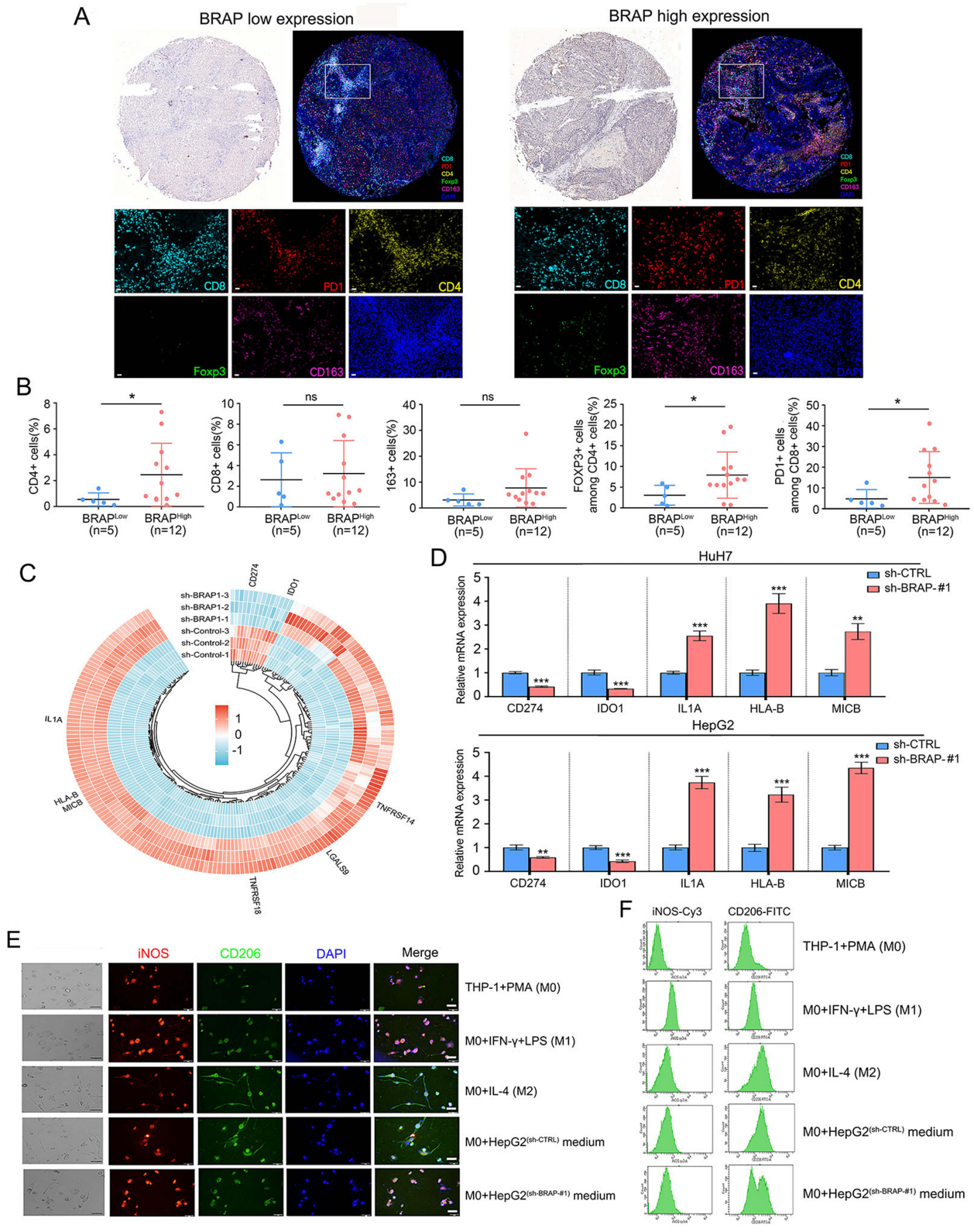

Figure 9 Effects of BRAP on the regulation of the immunosuppressive tumor microenvironment in HCC. (**A**) Representative image of mfIHC in low BRAP expression (n=7) and high BRAP expression (n=10) HCC tissues. mfIHC revealed the protein expression and localization of CD4 (yellow), CD8 (cyan), CD163 (purple), Foxp3 (green), and PD-1 (red) in HCC tissues, with DAPI stained cell nucleus shown in blue (scale bar=20 μm). (**B**) Quantification of CD4+ T cells, CD8+ T cells, CD163+ macrophages, CD4+Foxp3+ T cells, and PD-1+CD8+ T cells. (**C**) Heatmap depicting DEGs related to the immune response. (**D**) qRT–PCR validation of genes, including CD274, IDO1, IL1A, HLA-B, and MICB. (**E** and **F**) Analysis of macrophage polarization via immunofluorescence and flow cytometry was performed under co-culture with HepG2 cells (sh-BRAP or sh-CTRL). Macrophages were stimulated with either IFN-γ + LPS (to induce M1 polarization) or IL-4 (to induce M2 polarization), and the following surface markers were assessed: CD206 (M2 marker) and iNOS (M1 marker). Data are represented as mean ± SD and representative of three independent experiments. ns: $P>0.05$;*$P \leq 0.05$; **$P < 0.01$; ***$P < 0.001$.

https://doi.org/10.2147/JHC.S547105

BRAP-Mediated Regulation of Immunosuppressive Tumor Microenvironment Composition and Immunotherapy in HCC Patients

Previous RNA-seq data, coupled with pathway enrichment analyses, have unveiled BRAP's intricate involvement in immune-related pathways, encompassing leukocyte migration, cytokine production, and inflammatory responses. Herein, we evaluated the association between BRAP and these pathways within the context of HCC. Our exploration commenced with the TIMER database, which facilitated an insightful analysis of immune cell infiltration levels in HCC tissues exhibiting high versus low BRAP expression. Intriguingly, tissues with high-BRAP expression exhibited a marked increase in the proportion of type 2 T helper (Th2) cells, in stark contrast to a decline in the infiltration of activated natural killer (NK) cells and neutrophils, when compared to their low-BRAP counterparts (Figure S5A-B). Further analysis revealed a positive correlation between BRAP expression and activated CD4+ T-cell infiltration. Conversely, there was a negative correlation with the infiltration of activated CD8+ T cells, neutrophils, and NK cells (Figure S5C).

Recent studies have highlighted the pivotal role of high immune checkpoint genes (ICGs) expression in enhancing immune escape within the tumor microenvironment. Consequently, drugs targeting these ICGs are currently the subject of intense clinical and preclinical research.[22,23] Motivated by these advancements, we embarked on an analysis to elucidate the relationship between BRAP and ICGs expression. Our results indicated that high BRAP expression was associated with elevated levels of ICGs, including PDCD1 (PD-1), CTLA-4, LAG3, TIGIT, and HAVCR2 (TIM3) in HCC tissues (Figure S5D-E). These findings not only deepen our understanding of BRAP's role in modulating the immunosuppressive tumor microenvironment but also hint at potential therapeutic implications for immunotherapy in HCC patients.

On the basis of the above findings, we conducted an mfIHC analysis to quantitatively evaluate the infiltration patterns of various immune cells within the tumor microenvironment (Figure 9A). Our initial observations revealed a marked elevation in CD4+ T-cell infiltration levels within HCC tissues exhibiting high BRAP expression. Conversely, no statistically significant variations were discernible in the infiltration levels of CD8+ T cells or CD163+ macrophages. Intriguingly, a more pronounced presence of CD4+FoxP3+ T cells (regulatory T cells, Tregs) and CD8+PD-1+ T cells was evident in samples belonging to the high-BRAP expression group, in comparison to those in the low-BRAP expression group (Figure 9B). To explore how BRAP exerts its immunosuppressive functions, we conducted a comprehensive screen for DEGs related to immunity in HepG2 cells, comparing the sh-BRAP group with the sh-CTRL group. As depicted in Figure 9C, the knockdown of BRAP had a significant impact on the expression of several immune-related genes, including CD274 (PDL1), IDO1, IL1A, HLA-B, and MICB. Notably, CD274 and IDO1 are well-established inhibitors of T-cell activation, known to facilitate tumor evasion from immune surveillance.[23–25] Conversely, IL-1A functions as a cytokine that augments antitumor immunity by recruiting antigen-presenting cells to activate tumor-specific CD4+ and CD8+ T cells.[26,27] HLA-B and MICB play pivotal roles in antigen presentation to T cells and the initiation of adaptive immune responses.[28,29] Consistent with these observations, qRT-PCR analysis further corroborated the significant downregulation of CD274 and IDO1 expression in HepG2 cells following BRAP knockdown. Additionally, the knockdown of BRAP led to a marked upregulation in the expression of IL-1A, HLA-B, and MICB (Figure 9D). To establish causal mechanisms of BRAP-mediated immune evasion, we conducted key functional experiments. First, THP-1 monocytes were differentiated into M0 macrophages using PMA. Subsequently, the differentiated M0 macrophages were co-cultured with HepG2 cells (sh-BRAP or sh-CTRL) for 7 days to allow for intercellular interaction and potential modulation of macrophage polarization. On day 7 of the co-culture period, adherent macrophage cells were carefully collected to isolate the macrophage population of interest. To assess the impact of BRAP on macrophage polarization, we analysis using immunofluorescence (IF) staining and flow cytometry revealed that co-culturing M0 macrophages with sh-BRAP HepG2 cells significantly reduced the number of M2-polarized macrophages compared to the sh-CTRL group (Figure 9E and F). Collectively, these findings suggest that BRAP may contribute to the formation of an immunosuppressive tumor microenvironment in HCC by facilitating the infiltration of immunosuppressive cells, upregulating ICG expression, and promoting M2 macrophage populations.

Currently, ICB therapy stands as a pivotal facet within the realm of cancer immunotherapy. The existing ICB therapies primarily focus on reversing T-cell exhaustion and augmenting their antitumor capabilities. Tumor mutational burden (TMB) has been established as a predictor of enhanced ICB therapy efficacy, given its ability to generate novel antigens that attract CD8+ T cells into tumor tissue, thereby eliciting cytotoxic effects.[30,31] Consequently, we analyzed differences in TMB between high- and low-BRAP-expressing HCC tissues. The results revealed that a statistically significant increase in TMB among patients with elevated BRAP expression compared to those with lower levels. Furthermore, our analysis revealed that the p53 mutation frequency was significantly greater in the high-BRAP-expressing cohort than in the low-BRAP-expressing cohort (Figure S6). Collectively, these results underscore the intricate association between immune evasion and therapeutic responsiveness in HCC with BRAP enrichment.

Discussion

BRAP, a BRCA1-associated protein, exhibits aberrantly upregulation in various malignancies. Previous research has revealed that BRAP plays a carcinogenic role in the pathogenesis of HCC, with its expression level positively correlating with the infiltration of immunosuppressive cells.[10] However, the precise mechanisms by which BRAP influences HCC progression and its potential value as a therapeutic target remain unclear. To elucidate the underlying mechanisms by which BRAP drives HCC tumorigenesis and promotes immune evasion, we conducted a series of investigations, encompassing bioinformatics analyses, clinical feature assessment, and cytological experiments.

In this study, we first revealed that BRAP gene expression is significantly elevated in HCC cells and tissues compared with the corresponding normal liver counterparts. Notably, a heightened expression of BRAP was discernible in HCC tissues that correlated with advanced pathological grades and clinical stages. Furthermore, survival analysis pointed towards a poor prognosis for HCC patients exhibiting high BRAP expression levels. BRAP's prognostic significance was consistently replicated across our clinical cohort and independent TCGA and ICGC datasets, confirming its robustness as an HCC prognostic marker. To substantiate the impact of BRAP on HCC cell proliferation, lentiviral transduction was employed, facilitating both in vivo and in vitro assessments. To delve deeper into the biological functions associated with BRAP in HCC cells, we conducted GO and GSEA, leveraging our RNA-seq data alongside TCGA datasets. Our findings showed that genes co-expressed with BRAP were primarily involved in regulating cell cycle processes and MAPK/ERK signaling pathways. It is noteworthy that disruptions in the cell cycle are closely linked to the cell proliferation and progression of HCC.[32,33] Moreover, prior research conducted in our laboratory has confirmed that knockout of BRAP in neural progenitor cells (NPCs) results in cell cycle arrest.[34] Consistent with these preceding findings, our results indicated that BRAP knockdown led to delayed cell cycle progression and a reduction in the S phase population. Intriguingly, Huh7 and HepG2 cells exhibited distinct cell cycle distributions following BRAP knockdown. Specifically, inhibiting BRAP in Huh7 cells significantly increased the population of cells in the G2/M phase, compared to HepG2 cells. Western blotting analysis further revealed that silencing BRAP resulted in the upregulation of p21 expression, while concurrently downregulating Cyclin D1 and CDK4 levels in HepG2 cells. These Western blotting results align with previous flow cytometric analyses of the cell cycle. These observations hint at a potential association between the mutation status of the p53 gene in Huh7 (p53Y220C) and HepG2 (WT-p53) cells and their cell cycle distribution. Mutant p53 not only loses the tumor suppressor activity that characterizes wild-type p53 but also its inhibitory effect on p21, thereby potentially further promoting the malignant proliferation of tumor cells.[35–37] Thus, our findings contribute to a deeper understanding of the role of BRAP in HCC and its potential as a therapeutic target, warranting further exploration.

Given the profound enrichment of MAPK/ERK signaling pathways evident in our analyses, we delved deeper into the potential regulatory role of BRAP within these pathways. Notably, aberrant activation of the MAPK/ERK signaling pathway has been implicated in tumorigenesis and tumor progression, as documented in numerous studies.[19,38] Prior research has further demonstrated that downregulation of BRAP in gastric cancer cells leads to decreased phosphorylation levels of ERK, ultimately suppressing cancer cell proliferation, migration, and EMT.[11] In accordance with these findings, our data also confirmed that silencing BRAP inhibits cellular proliferation by inducing cell cycle arrest via suppression of MAPK/ERK signaling pathway activation.

HCC is characterized by marked heterogeneity at both molecular and tissue levels,[39] along with a similarly intricate immune microenvironment. Numerous studies have underscored the critical role of tumor-infiltrating lymphocytes and their activation status within the immune microenvironment, closely linking them to tumorigenesis and tumor progression.[40–43] Recent advancements in single-cell genomics have enriched our understanding of the antitumor effects of various immune cell components within tumor tissues. Several studies have revealed a reduced presence of cytotoxic CD8+ T cells in HCC tissues, accompanied by a significant increase in dysfunctional and exhausted CD8+ T cells, Tregs, and tumor-associated macrophages (TAMs).[20,44] Consequently, the immunosuppressive microenvironment of HCC tissues formed by these cells, plays a pivotal role in inducing tumor immune escape and promoting malignant tumor progression.[21] Variations in immune cell infiltration induced by cytokines and chemokines, have also been shown to influence the establishment of an immunosuppressive microenvironment in HCC.[45,46] Our previous studies, conducted in a mouse model of BRAP conditional knockout ($BRAP^{cKO}$) neuronal precursors, revealed that a substantial number of cytokines and chemokines released by senescent neurons contribute to neuroinflammation in the cortex.[47] Furthermore, our RNA sequencing data and pathway enrichment analysis indicated that BRAP is involved in immune-related pathways, encompassing leukocyte migration, cytokine production, and the inflammatory response. Given this background, we initially investigated whether BRAP expression correlated with the level of immune infiltration using the ESTIMATE algorithm. The results indicated a significant increase in Th2 cells in the high-BRAP-expressing group, accompanied by a decrease in activated NK cells and neutrophils. Further analysis unveiled a positive correlation between BRAP expression and the infiltration of activated CD4+ T cells, and a negative correlation with CD8+ T cells, NK cells, and Th1 cells.

It is noteworthy that naive CD4+ T cells can differentiate into Th1, Th2, Th17, and Treg cells. During the tumor immune response, Th1 cells activate CD8+ T and NK cells to eliminate tumor cells. Conversely, Th2 cells facilitate the differentiation and proliferation of immunosuppressive populations, such as TAMs and myeloid-derived suppressor cells (MDSCs). These findings align with recent reports indicating an imbalance between Th1 and Th2 cell subsets in HCC tissues, favoring Th2 polarization. This shift promotes immune evasion by tumor cells and restricts antitumor immune responses.[48,49] We subsequently explored the correlation between BRAP expression and the expression of ICGs. Studies on immune-related functions have shown that the expression levels of ICGs are closely associated with immune escape and cancer prognosis.[22,23,50] Our analysis revealed that high BRAP expression was linked to increased levels of ICGs, such as PD-1, CTLA-4, LAG3, TIM3, and IL10RB in HCC tissues. Notably, drugs targeting these ICGs are currently under clinical or preclinical development.[4,51–54] To further evaluate the infiltration of various immune cell types, we conducted mfIHC analysis. Our findings demonstrated that CD4+ T-cell infiltration levels were significantly elevated in HCC tissues with high BRAP expression. However, no statistically significant difference was observed in CD8+ T-cell or CD163+ macrophage infiltration. Furthermore, the presence of CD4+FoxP3+ T cells and CD8+PD-1+ T cells was notably higher in the high-BRAP group compared to the low-BRAP group. The qRT-PCR assay subsequently validated these findings by identifying DEGs related to immunity. BRAP knockdown significantly decreased the expression of CD274 and IDO1, while increasing the expression of IL1A, HLA-B, and MICB. Therefore, silencing BRAP ultimately enhances lymphocyte cytotoxicity while inhibiting lymphocyte tolerance in HCC. To establish causal mechanisms of BRAP-mediated immune evasion, we performed macrophage-tumor co-culture experiments. THP-1-derived M0 macrophages were co-cultured with HepG2 cells (sh-BRAP vs sh-CTRL). Immunofluorescence and flow cytometry revealed significantly fewer M2-polarized macrophages when co-cultured with sh-BRAP HepG2 cells versus sh-CTRL. These demonstrates that BRAP drives immunosuppression in HCC by promoting both immunosuppressive cell infiltration and M2 macrophage polarization. While these data establish functional causality, T-cell suppression assays will further validate these mechanisms in future work.

Increased TMB has emerged as a promising biomarker in predicting the enhanced efficacy of ICB therapy. It generates novel antigens capable of recruiting specific CD8+ T cells into tumor tissue, thereby exerting potent cytotoxic effects. Consequently, we utilized Maftools to dissect the disparities in TMB based on BRAP expression levels in HCC samples. Our study unveiled a significant elevation in TMB among patients with high BRAP expression compared to those with low expression. Furthermore, the mutation frequency of p53 was notably higher in the high BRAP expression group than in the low expression group. Prior research has substantiated that HCC patients with p53 mutations exhibit

augmented immunogenicity and favorable objective responses, accompanied by improved survival rates, subsequent to ICB treatment.[55,56] These findings suggest that HCC patients with high BRAP expression are more amenable to ICB therapy.

Conclusion

Our study demonstrated the BRAP expression is significantly upregulated in HCC tissues and is associated with advanced pathological grades and poor prognosis. The knockdown of BRAP markedly reduced HCC cell viability both in vitro and in vivo. Furthermore, silencing BRAP inhibited cellular proliferation by inducing cell cycle arrest via the suppression of MAPK/ERK signaling pathway activation. BRAP-enriched tumors are characterized by high infiltration of immunosuppressive cells, upregulated expression of ICGs, and enhanced M2 macrophage polarization. However, elevated BRAP expression led to increased tumor TMB, thereby enhancing the efficacy of ICB therapy in patients with HCC. Therefore, BRAP has the potential to be a biomarker for the diagnosis and prognosis of HCC. From the perspective of precision medicine, the detection of BRAP expression can more accurately identify the population that would benefit from immunotherapy.

Abbreviations

AUC, area under the curve; DEGs, differential expression of genes; DFS, disease-free survival; EdU, 5-Ethynyl-2′-deoxyuridine assay; GEO, Gene Expression Omnibus; GSEA, gene set enrichment analysis; GO, Gene Ontology; HCC, hepatocellular carcinoma; ICB, immune checkpoint blockade; ICGs, immune checkpoint genes; mfIHC, multiplex immunofluorescence; OS, overall survival; PFS, progression-free survival; PVTT, portal vein tumor thrombus; qRT-PCR, quantitative real-time polymerase chain reaction; TMB, tumor mutation burden.

Data Sharing Statement

The datasets used and materials used in this study are available from the corresponding author (Shundong Cang) upon reasonable request.

Ethics Approval and Consent to Participate

Studies using human tissues were approved by the Human Research Ethics Committees of Shanghai Outdo Biotech Company (Shanghai, China, SHYJS-CP-1601006 and SHYJS-CP-2206007) in agreement with the guidelines set forth by the Declaration of Helsinki. Written informed consent was obtained from all patients whose tissues were used in this study. Studies on animals were conducted in accordance with relevant guidelines and regulations and were approved by the Animal Research Ethics Committee of Zhengzhou University (Zhengzhou, China; ZZU-LAC20220909).

Consent for Publication

All involved parties consent to publication.

Funding

This study was supported by the Natural Science Foundation of China (No.82372896 and 81872420), Foundation of Cancer Biology State Key Laboratory (No. CBSKL2022ZDKF12), Key Scientific Research Foundation of Henan Educational Committee (No. 24A310018), and Key Research and Development Project of Henan Province (No.231111311900).

Disclosure

The authors report no conflicts of interest in this work.

References

1. Siegel RL, Giaquinto AN, Jemal A. Cancer statistics, 2024. *CA Cancer J Clin*. 2024;74(1):12–49. doi:10.3322/caac.21820

2. Vitale A, Trevisani F, Farinati F, Cillo U. Treatment of hepatocellular carcinoma in the precision medicine era: from treatment stage migration to therapeutic hierarchy. *Hepatology*. 2020;72(6):2206–2218. doi:10.1002/hep.31187
3. Chidambaranathan-Reghupaty S, Fisher PB, Sarkar D. Hepatocellular carcinoma (HCC): epidemiology, etiology and molecular classification. *Adv Cancer Res*. 2021;149:1–61. doi:10.1016/bs.acr.2020.10.001
4. Kole C, Charalampakis N, Tsakatikas S, et al. Immunotherapy for hepatocellular carcinoma: a 2021 update. *Cancers*. 2020;12(10):2859. doi:10.3390/cancers12102859
5. Li S, Ku CY, Farmer AA, Cong YS, Chen CF, Lee WH. Identification of a novel cytoplasmic protein that specifically binds to nuclear localization signal motifs. *J Biol Chem*. 1998;273(11):6183–6189. doi:10.1074/jbc.273.11.6183
6. D'Amora DR, Hu Q, Pizzardi M, Kubiseski TJ. BRAP-2 promotes DNA damage induced germline apoptosis in C. elegans through the regulation of SKN-1 and AKT-1. *Cell Death Differ*. 2018;25(7):1276–1288. doi:10.1038/s41418-017-0038-7
7. Fatima S, Wagstaff KM, Loveland KL, Jans DA. Interactome of the negative regulator of nuclear import BRCA1-binding protein 2. *Sci Rep*. 2015;5:9459. doi:10.1038/srep09459
8. Matheny SA, Chen C, Kortum RL, Razidlo GL, Lewis RE, White MA. Ras regulates assembly of mitogenic signalling complexes through the effector protein IMP. *Nature*. 2004;427(6971):256–260. doi:10.1038/nature02237
9. Asada M, Ohmi K, Delia D, et al. Brap2 functions as a cytoplasmic retention protein for p21 during monocyte differentiation. *Mol Cell Biol*. 2004;24(18):8236–8243. doi:10.1128/mcb.24.18.8236-8243.2004
10. Ju Q, Li XM, Zhang H, Zhao YJ. BRCA1-associated protein is a potential prognostic biomarker and is correlated with immune infiltration in liver hepatocellular carcinoma: a pan-cancer analysis. *Front Mol Biosci*. 2020;7:573619. doi:10.3389/fmolb.2020.573619
11. Wei X, Liu X, Liu H, et al. BRCA1-associated protein induced proliferation and migration of gastric cancer cells through MAPK pathway. *Surg Oncol*. 2020;35:191–199. doi:10.1016/j.suronc.2020.08.007
12. Yin WJ, Li LM, Wang L, et al. Correlation between BRAP expression and prognosis of patients with laryngeal squamous cell carcinoma. *Lin Chuang Er Bi Yan Hou Tou Jing Wai Ke Za Zhi*. 2019;33(11):1081–1084. doi:10.13201/j.issn.1001-1781.2019.11.018
13. Zhao Y, Wei L, Shao M, et al. BRCA1-associated protein increases invasiveness of esophageal squamous cell carcinoma. *Gastroenterology*. 2017;153(5):1304–1319.e5. doi:10.1053/j.gastro.2017.07.042
14. Mayakonda A, Lin DC, Assenov Y, Plass C, Koeffler HP. Maftools: efficient and comprehensive analysis of somatic variants in cancer. *Genome Res*. 2018;28(11):1747–1756. doi:10.1101/gr.239244.118
15. Lu Y, Yang A, Quan C, et al. A single-cell atlas of the multicellular ecosystem of primary and metastatic hepatocellular carcinoma. *Nat Commun*. 2022;13(1):4594. doi:10.1038/s41467-022-32283-3
16. Guo Y, Pan Q, Zhang J, et al. Functional and clinical evidence that TAZ is a candidate oncogene in hepatocellular carcinoma. *J Cell Biochem*. 2015;116(11):2465–2475. doi:10.1002/jcb.25117
17. Murray PJ. Macrophage Polarization. *Annu Rev Physiol*. 2017;79:541–566. doi:10.1146/annurev-physiol-022516-034339
18. Xie B, Wang S, Jiang N, Li JJ. Cyclin B1/CDK1-regulated mitochondrial bioenergetics in cell cycle progression and tumor resistance. *Cancer Lett*. 2019;443:56–66. doi:10.1016/j.canlet.2018.11.019
19. Ullah R, Yin Q, Snell AH, Wan L. RAF-MEK-ERK pathway in cancer evolution and treatment. *Semin Cancer Biol*. 2022;85:123–154. doi:10.1016/j.semcancer.2021.05.010
20. Zheng C, Zheng L, Yoo JK, et al. Landscape of infiltrating T cells in liver cancer revealed by single-cell sequencing. *Cell*. 2017;169(7):1342–1356.e16. doi:10.1016/j.cell.2017.05.035
21. Kurebayashi Y, Ojima H, Tsujikawa H, et al. Landscape of immune microenvironment in hepatocellular carcinoma and its additional impact on histological and molecular classification. *Hepatology*. 2018;68(3):1025–1041. doi:10.1002/hep.29904
22. Datar I, Sanmamed MF, Wang J, et al. Expression analysis and significance of PD-1, LAG-3, and TIM-3 in human non-small cell lung cancer using spatially resolved and multiparametric single-cell analysis. *Clin Cancer Res*. 2019;25(15):4663–4673. doi:10.1158/1078-0432.Ccr-18-4142
23. Gibney GT, Weiner LM, Atkins MB. Predictive biomarkers for checkpoint inhibitor-based immunotherapy. *Lancet Oncol*. 2016;17(12):e542–e551. doi:10.1016/s1470-2045(16)30406-5
24. Melaiu O, Lucarini V, Giovannoni R, Fruci D, Gemignani F. News on immune checkpoint inhibitors as immunotherapy strategies in adult and pediatric solid tumors. *Semin Cancer Biol*. 2022;79:18–43. doi:10.1016/j.semcancer.2020.07.001
25. Tang K, Wu YH, Song Y, Yu B. Indoleamine 2,3-dioxygenase 1 (IDO1) inhibitors in clinical trials for cancer immunotherapy. *J Hematol Oncol*. 2021;14(1):68. doi:10.1186/s13045-021-01080-8
26. Song X, Voronov E, Dvorkin T, et al. Differential effects of IL-1 alpha and IL-1 beta on tumorigenicity patterns and invasiveness. *J Immunol*. 2003;171(12):6448–6456. doi:10.4049/jimmunol.171.12.6448
27. Krishnamohan M, Kaplanov I, Maudi-Boker S, et al. Tumor cell-associated IL-1α affects breast cancer progression and metastasis in mice through manipulation of the tumor immune microenvironment. *Int J Mol Sci*. 2024;25(7):3950. doi:10.3390/ijms25073950
28. Ferrari de Andrade L, Kumar S, Luoma AM, et al. Inhibition of MICA and MICB shedding elicits NK-cell-mediated immunity against tumors resistant to cytotoxic T cells. *Cancer Immunol Res*. 2020;8(6):769–780. doi:10.1158/2326-6066.Cir-19-0483
29. Badrinath S, Dellacherie MO, Li A, et al. A vaccine targeting resistant tumours by dual T cell plus NK cell attack. *Nature*. 2022;606(7916):992–998. doi:10.1038/s41586-022-04772-4
30. Jardim DL, Goodman A, De melo gagliato D, Kurzrock R. The challenges of tumor mutational burden as an immunotherapy biomarker. *Cancer Cell*. 2021;39(2):154–173. doi:10.1016/j.ccell.2020.10.001
31. Bareche Y, Kelly D, Abbas-Aghababazadeh F, et al. Leveraging big data of immune checkpoint blockade response identifies novel potential targets. *Ann Oncol*. 2022;33(12):1304–1317. doi:10.1016/j.annonc.2022.08.084
32. Kohrman AQ, Matus DQ. Divide or conquer: cell cycle regulation of invasive behavior. *Trends Cell Biol*. 2017;27(1):12–25. doi:10.1016/j.tcb.2016.08.003
33. Wu MY, Yiang GT, Cheng PW, Chu PY, Li CJ. Molecular targets in hepatocarcinogenesis and implications for therapy. *J Clin Med*. 2018;7(8):213. doi:10.3390/jcm7080213
34. Lanctot AA, Guo Y, Le Y, Edens BM, Nowakowski RS, Feng Y. Loss of Brap results in premature G1/S phase transition and impeded neural progenitor differentiation. *Cell Rep*. 2017;20(5):1148–1160. doi:10.1016/j.celrep.2017.07.018

35. Walker DR, Bond JP, Tarone RE, et al. Evolutionary conservation and somatic mutation hotspot maps of p53: correlation with p53 protein structural and functional features. *Oncogene*. 1999;18(1):211–218. doi:10.1038/sj.onc.1202298
36. Thangavelu L, Altamimi ASA, Ghaboura N, et al. Targeting the p53-p21 axis in liver cancer: Linking cellular senescence to tumor suppression and progression. *Pathol Res Pract*. 2024;263:155652. doi:10.1016/j.prp.2024.155652
37. Xiao BD, Zhao YJ, Jia XY, Wu J, Wang YG, Huang F. Multifaceted p21 in carcinogenesis, stemness of tumor and tumor therapy. *World J Stem Cells*. 2020;12(6):481–487. doi:10.4252/wjsc.v12.i6.481
38. Moon H, Ro SW. MAPK/ERK signaling pathway in hepatocellular carcinoma. *Cancers*. 2021;13(12). doi:10.3390/cancers13123026
39. Calderaro J, Ziol M, Paradis V, Zucman-Rossi J. Molecular and histological correlations in liver cancer. *J Hepatol*. 2019;71(3):616–630. doi:10.1016/j.jhep.2019.06.001
40. Dong C. Cytokine regulation and function in T cells. *Annu Rev Immunol*. 2021;39:51–76. doi:10.1146/annurev-immunol-061020-053702
41. Farhood B, Najafi M, Mortezaee K. CD8(+) cytotoxic T lymphocytes in cancer immunotherapy: a review. *J Cell Physiol*. 2019;234(6):8509–8521. doi:10.1002/jcp.27782
42. Lin B, Du L, Li H, Zhu X, Cui L, Li X. Tumor-infiltrating lymphocytes: warriors fight against tumors powerfully. *Biomed Pharmacother*. 2020;132:110873. doi:10.1016/j.biopha.2020.110873
43. Sia D, Jiao Y, Martinez-Quetglas I, et al. Identification of an immune-specific class of hepatocellular carcinoma, based on molecular features. *Gastroenterology*. 2017;153(3):812–826. doi:10.1053/j.gastro.2017.06.007
44. Chew V, Lai L, Pan L, et al. Delineation of an immunosuppressive gradient in hepatocellular carcinoma using high-dimensional proteomic and transcriptomic analyses. *Proc Natl Acad Sci U S A*. 2017;114(29):E5900–e5909. doi:10.1073/pnas.1706559114
45. Commins SP, Borish L, Steinke JW. Immunologic messenger molecules: cytokines, interferons, and chemokines. *J Allergy Clin Immunol*. 2010;125 (2 Suppl 2):S53–72. doi:10.1016/j.jaci.2009.07.008
46. Propper DJ, Balkwill FR. Harnessing cytokines and chemokines for cancer therapy. *Nat Rev Clin Oncol*. 2022;19(4):237–253. doi:10.1038/s41571-021-00588-9
47. Guo Y, Chomiak AA, Hong Y, et al. Histone H2A ubiquitination resulting from Brap loss of function connects multiple aging hallmarks and accelerates neurodegeneration. *iScience*. 2022;25(7):104519. doi:10.1016/j.isci.2022.104519
48. Zamarron BF, Chen W. Dual roles of immune cells and their factors in cancer development and progression. *Int J Biol Sci*. 2011;7(5):651–658. doi:10.7150/ijbs.7.651
49. Ge J, Yin X, Chen L. Regulatory T cells: masterminds of immune equilibrium and future therapeutic innovations. *Front Immunol*. 2024;15:1457189. doi:10.3389/fimmu.2024.1457189
50. Yoshida Y, Mikami N, Nakanishi Y, et al. Characterization of an expanded IL-10-producing-suppressive T cell population associated with immune tolerance. *Biol Pharm Bull*. 2021;44(4):585–589. doi:10.1248/bpb.b19-01072
51. Agdashian D, ElGindi M, Xie C, et al. The effect of anti-CTLA4 treatment on peripheral and intra-tumoral T cells in patients with hepatocellular carcinoma. *Cancer Immunol Immunother*. 2019;68(4):599–608. doi:10.1007/s00262-019-02299-8
52. Dougall WC, Kurtulus S, Smyth MJ, Anderson AC. TIGIT and CD96: new checkpoint receptor targets for cancer immunotherapy. *Immunol Rev*. 2017;276(1):112–120. doi:10.1111/imr.12518
53. Kandel S, Adhikary P, Li G, Cheng K. The TIM3/Gal9 signaling pathway: An emerging target for cancer immunotherapy. *Cancer Lett*. 2021;510:67–78. doi:10.1016/j.canlet.2021.04.011
54. Andrews LP, Marciscano AE, Drake CG, Vignali DA. LAG3 (CD223) as a cancer immunotherapy target. *Immunol Rev*. 2017;276(1):80–96. doi:10.1111/imr.12519
55. Calderaro J, Couchy G, Imbeaud S, et al. Histological subtypes of hepatocellular carcinoma are related to gene mutations and molecular tumour classification. *J Hepatol*. 2017;67(4):727–738. doi:10.1016/j.jhep.2017.05.014
56. Chakraborty E, Sarkar D. Emerging therapies for hepatocellular carcinoma (HCC). *Cancers*. 2022;14(11):2798. doi:10.3390/cancers14112798